Research Square

Preprints are preliminary reports that have not undergone peer review.
They should not be considered conclusive, used to inform clinical practice,
or referenced by the media as validated information.

Oxidative Stress, Mitochondrial Transport and Tubulin Code Remodeling Underlie Oxaliplatin-Induced Peripheral Neuropathy

Maria Elena Pero

mepero@unina.it

University of Naples Federico II

Cristina Meregalli

University of Milano-Bicocca

Silvia Giatti

University of Milan

Farihah Chowdhury

Columbia University

Caecilia Lee

Columbia University

Patricia Morcillo

Karolinska Institutet

Alessia Chiorazzi

University of Milano-Bicocca

Annalisa Canta

University of Milano-Bicocca

Paola Alberti

University of Milano-Bicocca

Valentina Alda Carozzi

University of Milano-Bicocca

Eleonora Pozzi

University of Milano-Bicocca

Pietro Lombardi

University of Naples Federico II

Silvia Diviccaro

Saarland University

Roberto Cosimo Melcangi

University of Milan

Francesca Bartolini

Columbia University

Guido Cavaletti

University of Milano-Bicocca

Research Article

Keywords: Chemotherapy-induced peripheral neuropathy (CIPN), Oxaliplatin, Tubulin code, Polyglutamylation, Mitochondrial dysfunction, Organelle trafficking

Posted Date: November 24th, 2026

DOI: https://doi.org/10.21203/rs.3.rs-11567143/v1

License: This work is licensed under a Creative Commons Attribution 4.0 International License. Read Full License

Additional Declarations: No competing interests reported.

Title: Oxidative Stress, Mitochondrial Transport and Tubulin Code Remodeling Underlie Oxaliplatin-Induced Peripheral Neuropathy

Running Title: *Mitochondrial And Tubulin Code Remodeling In Oxaliplatin Neuropathy*

Oxaliplatin and 5-fluorouracil share early mitochondrial bioenergetic dysfunction, but only oxaliplatin triggers oxidative stress, tubulin polyglutamylation, altered mitochondrial and lysosomal trafficking, and subsequent axonal degeneration. These findings identify cytoskeletal and organelle-transport remodeling as distinctive mechanisms linking mitochondrial stress to oxaliplatin-induced peripheral neuropathy.

[1,2] Pero ME.*°, [3,4]Meregalli C.°, [5]Giatti S., [1]Chowdhury F., [1]Lee C., [6]Morcillo P., [3,4]Chiorazzi A., [3,4]Canta A., [3,4]Alberti P, [3,4]Carozzi V.A., [3,4]Pozzi E., [2]Lombardi P., [7]Diviccaro S., [5]Melcangi R.C., [1]Bartolini F. †* and [3,4]Cavaletti G. †*

[1]Department of Pathology and Cell Biology, 630w, 168th street, P&S 14-401, 10032, New York, USA; [2]Department of Veterinary Medicine and Animal Production, University of Naples, Federico II, Naples, via Delpino, 1, 80130, Naples, Italy; [3]Experimental Neurology Unit, School of Medicine and Surgery, University of Milano-Bicocca, Via Cadore 48, 20900, Monza, Italy
[4]NeuroMI (Milan Center for Neuroscience), University of Milano-Bicocca, Monza, Italy. [5]Department of Pharmacological and Biomolecular Sciences "Rodolfo Paoletti", University of Milan, Milan, Italy; [6]Department of Neurobiology, Care Sciences and Society, Division of Neurogeriatrics, Center for Alzheimer Research. Karolinska Institutet, Visionsgatan 4, 171 64 Solna, Sweden; [7]Saarland University Medical Center, Department of Medicine II, Kirrberger Straße 100, Homburg, Germany

*Corresponding Authors:
Francesca Bartolini fb2131@cumc.columbia.edu
630w, 168th street, P&S 14-401, 10032, New York, USA.

Guido Cavaletti guido.cavaletti@unimib.it
University of Milano-Bicocca, Via Cadore 48, 20900, Monza, Italy

Maria Elena Pero mepero@unina.it; mp3054@cumc.columbia.edu ;
University of Naples, Federico II, Naples, via Delpino, 1, 80130, Naples, Italy;
630w, 168th street, P&S 14-401, 10032, New York, USA.

†These authors contributed equally and share senior authorship.
°These authors contributed equally and share first authorship

Authors contact infomation and ORCID ID

Maria Elena Pero,
ORCID: 0000-0001-7262-6350
mepero@unina.it; mp3054@cumc.columbia.edu;
University of Naples Federico II, Italy; Columbia University, USA
Office phone +39 0812536103

Cristina Meregalli
ORCID 0000-0002-4281-4577
cristina.meregalli@unimib.it
University of Milano-Bicocca, Italy

Silvia Giatti
ORCID 0000-0001-7741-826X
silvia.giatti@unimi.it
University of Milan Italy

Farihah Chowdhury
ORCID: 0000-0001-8208-1710
fc2670@columbia.edu
Columbia University USA

Caecilia Lee
ORCID 0009-0002-1175-0686
cl4430@columbia.edu
Columbia University USA

Patricia Morcillo
ORCID 0000-0002-2175-4421
patricia.morcillo.garcia@ki.se
Karolinska Institutet, Sweden

Alessia Chiorazzi
ORCID 0000-0002-3469-1829
alessia.chiorazzi@unimib.it
University of Milano-Bicocca, Italy

Annalisa Canta
ORCID 0000-0003-4946-647X
annalisa.canta@unimib.it
University of Milano-Bicocca, Italy

Paola Alberti
ORCID 0000-0001-6106-6183
paola.alberti@unimib.it
University of Milano-Bicocca, Italy

Valentina Alda Carozzi
ORCID 0000-0003-0963-7107
valentina.carozzi1@unimib.it
University of Milano-Bicocca, Italy

Eleonora Pozzi
ORCID0000-0001-6438-286X
eleonora.pozzi@unimib.it
University of Milano-Bicocca, Italy

Pietro Lombardi

ORCID: 0000-0001-7876-8800
pietro.lombardi@unina.it
University of Naples Federico II, Italy

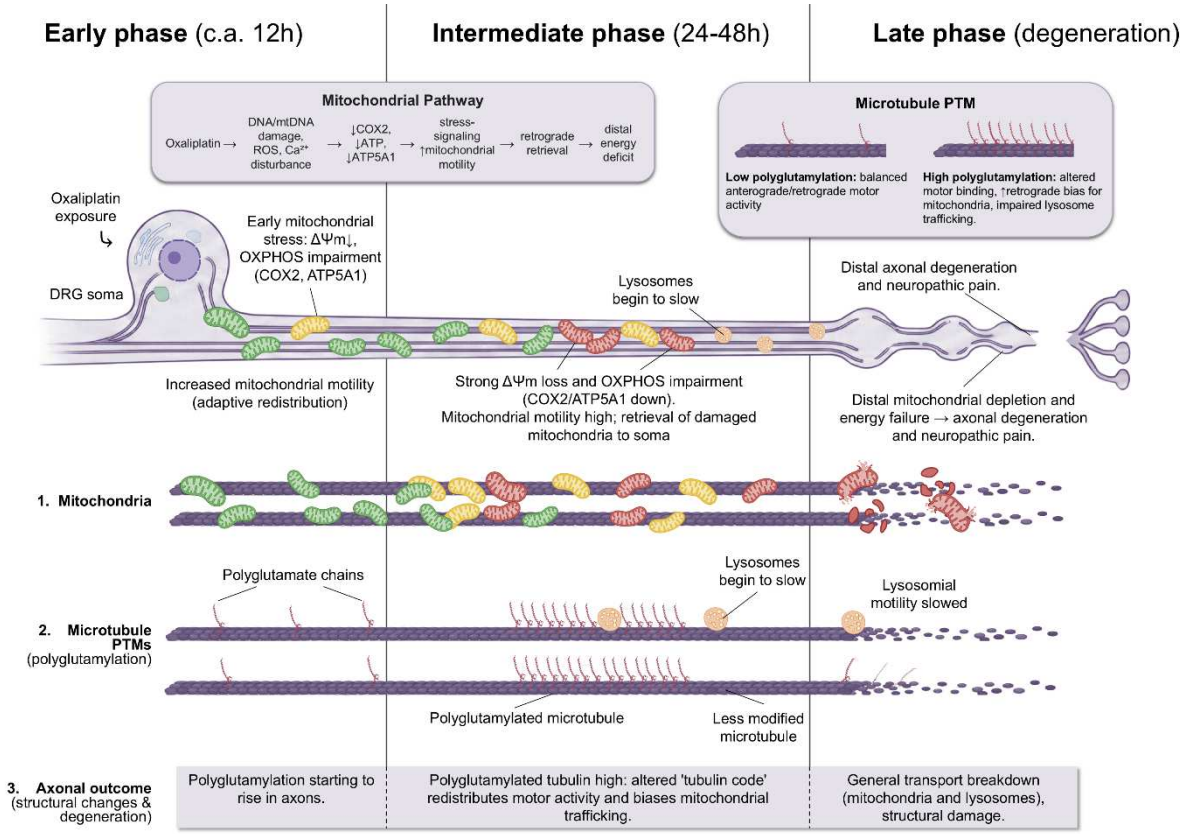
Silvia Diviccaro
ORCID 0000-0003-1454-2196
silvia.diviccaro@uks.eu
Saarland University Medical Center,Germany

Roberto C. Melcangi
ORCID 0000-0003-0861-8967
roberto.melcangi@unimi.it
University of Milan, Italy

Francesca Bartolini
ORCID 0000-0003-1048-622X
fb2131@cumc.columbia.edu
Columbia University USA
Office phone +1 212- 305-7299

Guido Cavaletti
ORCID 0000-0003-4128-2406
guido.cavaletti@unimib.it
University of Milano-Bicocca, Italy
Office phone + 39 02 6448 8039

GRAPHICAL ABSTRACT



Oxaliplatin induces early mitochondrial dysfunction (COX2/ATP5A1 loss, ΔΨm↓), increased and then retrograde-biased mitochondrial motility, and elevated tubulin polyglutamylation in sciatic nerve and DRG, which together drive progressive transport imbalance, distal mitochondrial depletion, and eventual axonal degeneration characteristic of CIPN.

Graphical Abstract. Proposed temporal model of oxaliplatin-induced peripheral neuropathy.

Schematic of oxaliplatin-induced progression in DRG neurons: early mitochondrial stress (~12 h) increases mitochondrial motility, followed at 24–48 h by tubulin polyglutamylation and impaired organelle trafficking (increased retrograde mitochondrial transport, reduced lysosomal motility). Ultimately, persistent dysfunction leads to distal mitochondrial depletion, axonal degeneration, and peripheral neuropathy. Created with BioRender.com. *Created with BioRender.com.*

ABSTRACT

Chemotherapy-induced peripheral neuropathy (CIPN) is a frequent, dose-limiting complication of anticancer therapies, yet the mechanisms distinguishing neurotoxic from non-neurotoxic agents remain poorly understood. Mitochondrial dysfunction is considered a central driver of CIPN, but its relationship with cytoskeletal remodeling, organelle trafficking, and axonal degeneration remains unclear. We compared oxaliplatin (Oxa), strongly associated with sensory neuropathy, with 5-fluorouracil (5-FU), rarely associated with peripheral neurotoxicity. Using in vivo rat models and primary adult dorsal root ganglion (DRG) neurons, we investigated oxidative stress, mitochondrial bioenergetics, tubulin post-translational modifications (PTMs), organelle trafficking, and axonal integrity. Chronic Oxa, but not 5-FU, induced sensory neuropathy characterized by cold hypersensitivity, reduced sensory nerve action potential amplitude, and intraepidermal nerve fiber loss. Oxa also increased DRG oxidative stress, impaired antioxidant defenses, and reduced mt-COX2

and ATP5A1 expression. In cultured sensory neurons, both agents induced mitochondrial depolarization and impaired oxidative phosphorylation, indicating that bioenergetic dysfunction is not unique to neurotoxic chemotherapy. However, only Oxa promoted progressive accumulation of polyglutamylated tubulin, while other tubulin PTMs remained unchanged. Oxa also selectively remodeled organelle trafficking, producing early changes in mitochondrial motility followed by increased retrograde transport and later lysosomal trafficking impairment. These alterations preceded overt neurite degeneration and were absent following 5-FU treatment. Thus, mitochondrial bioenergetic dysfunction represents a shared response to chemotherapy, whereas oxidative stress, organelle trafficking alterations, and selective tubulin-code remodeling distinguish Oxa neurotoxicity and may represent therapeutic targets for preserving neuronal homeostasis and preventing CIPN.
The raw data of the study are archived and available at https://doi.org/10.17632/pfb2cwpt5x.2

Keywords: Chemotherapy-induced peripheral neuropathy (CIPN); Oxaliplatin; Tubulin code; Polyglutamylation; Mitochondrial dysfunction; Organelle trafficking.

INTRODUCTION

Chemotherapy-induced peripheral neuropathy (CIPN) is one of the most common and debilitating adverse effects of anticancer treatment, frequently limiting the dose and duration of otherwise effective therapies (Park et al., 2013; Cavaletti and Marmiroli, 2010; Park et al., 2023). Depending on the chemotherapeutic agent, cumulative dose, and time of evaluation, CIPN affects approximately 30-70% of patients receiving neurotoxic chemotherapy. The incidence is particularly high following treatment with microtubule-targeting agents and platinum compounds. For example, paclitaxel induces peripheral neuropathy in up to 80% of treated patients (Seretny et al., 2014), bortezomib causes painful sensory neuropathy in 30-60% of cases (Cavaletti and Jakubowiak, 2010; Moreau et al., 2011), and oxaliplatin (Oxa) produces acute neuropathic symptoms in up to 90% of patients and persistent chronic neuropathy in approximately 30-50%, particularly after high cumulative doses (Argyriou et al., 2013; Lucchetta et al., 2012; Gamelin et al., 2002; Grothey, 2003; Starobova and Vetter, 2017).

Clinically, CIPN is characterized by a predominantly sensory axonopathy that manifests as pain, numbness, paresthesia, and loss of sensory function, profoundly affecting quality of life and frequently necessitating treatment modification or discontinuation. Despite its high prevalence and substantial clinical impact, no disease-modifying therapies are currently available, and management remains largely symptomatic. Over the past two decades, mitochondrial dysfunction has emerged as one of the leading mechanisms proposed to underlie CIPN, giving rise to the so-called *mitotoxicity hypothesis* (Bennett et al., 2014; Doyle and Salvemini, 2021). Structural and functional mitochondrial abnormalities have been consistently reported in experimental models of CIPN, particularly in dorsal root ganglion (DRG) neurons, which are especially vulnerable because of their high metabolic demand, long axons, and limited protection afforded by the blood nerve barrier (Zheng et al., 2011). Mitochondrial swelling, impaired oxidative phosphorylation, membrane depolarization, calcium dysregulation, and increased production of reactive oxygen species (ROS) have all been associated with neuronal dysfunction and progressive axonal injury (Flatters and Bennett, 2006).

Collectively, these observations support the concept that mitochondrial dysfunction is an early and important component of CIPN pathogenesis. Despite the substantial evidence supporting mitochondrial involvement, however, several fundamental questions remain unresolved. Most mechanistic studies have focused on chemotherapeutic agents that are intrinsically neurotoxic, making it difficult to distinguish cellular responses that represent general consequences of chemotherapeutic stress from those that specifically drive peripheral nerve degeneration.

Moreover, although mitochondrial dysfunction has been extensively characterized, the molecular events that connect early mitochondrial stress to disruption of axonal homeostasis remain poorly understood. In particular, how mitochondrial dysfunction relates to remodeling of the neuronal

cytoskeleton, intracellular organelle trafficking, and ultimately axonal degeneration has yet to be clearly established. Consistent with the mitotoxicity hypothesis, considerable effort has been devoted to developing therapeutic strategies aimed at preserving mitochondrial function or reducing oxidative stress in CIPN. A wide range of antioxidant and mitochondria-targeted interventions, including acetyl-L-carnitine (ALCAR), α-lipoic acid, and reactive oxygen and nitrogen species scavengers, have shown encouraging neuroprotective effects in experimental models (Ma et al., 2018; Flatters et al., 2015; Doyle et al., 2025). However, these promising preclinical observations have translated poorly into clinical practice. For example, acetyl-L-carnitine failed to prevent CIPN and, unexpectedly, was associated with worsening neuropathic symptoms in a randomized clinical trial (Hershman et al., 2013). Likewise, the superoxide dismutase mimetics mangafodipir and calmangafodipir initially demonstrated protective effects in preclinical studies and early clinical trials but ultimately failed to show consistent efficacy in larger randomized studies (Canta et al., 2020; Glimelius et al., 2017; Pfeiffer et al., 2022; Karlsson et al., 2023). These disappointing clinical outcomes suggest that mitochondrial dysfunction and oxidative stress, although important components of the neuronal response to chemotherapy, may not fully account for the transition from early cellular stress to irreversible axonal degeneration. Rather, they raise the possibility that additional downstream mechanisms determine whether metabolically stressed sensory neurons successfully adapt or instead progress toward degeneration. Identifying these mechanisms remains a major challenge in the field and is essential for developing disease-modifying therapies capable of preventing CIPN.

Among the cellular processes essential for maintaining neuronal homeostasis, intracellular organelle trafficking has emerged as a critical determinant of axonal function. Because axons can extend over remarkably long distances, the proper distribution of mitochondria, lysosomes, and other organelles requires efficient microtubule (MT) dependent transport. More than 90% of axonal mitochondria rely on MT tracks and their associated motor proteins to reach sites of high metabolic demand, maintain local ATP production, regulate calcium homeostasis, and support synaptic function (Malacrida et al., 2019; Pero et al., 2023). Consequently, disruption of intracellular trafficking can impair organelle positioning and quality-control mechanisms long before overt structural degeneration becomes apparent. Indeed, growing evidence indicates that defective organelle trafficking is a common feature of several neurodegenerative disorders and experimental models of CIPN. Altered mitochondrial distribution and motility can compromise mitochondrial positioning along the axon, thereby disrupting local energy homeostasis and contributing to progressive neuronal dysfunction (Doyle et al., 2021; Pero et al., 2021; Meregalli et al., 2022; Iseppon et al., 2026). (Doyle et al., 2021; Pero et al., 2021; Meregalli et al., 2022; Iseppon et al., 2026). Likewise, disruption of lysosomal transport compromises autophagic flux and intracellular quality-control pathways that are essential for maintaining neuronal integrity. Together, these observations suggest that altered organelle trafficking may represent a critical point at which early cellular stress is translated into progressive neuronal dysfunction and axonal degeneration.

Because intracellular organelle trafficking is critically dependent on the microtubule cytoskeleton, increasing attention has focused on the role of microtubule remodeling in CIPN.

Several classes of chemotherapeutic agents associated with CIPN, including taxanes, vinca alkaloids, bortezomib, and platinum compounds, directly or indirectly perturb microtubule organization and function (Gornstein and Schwarz, 2014; Geisler et al., 2016; Geisler, 2019; Wozniak et al., 2017; Pero et al., 2021; Chua et al., 2022; Iseppon et al., 2026). Beyond serving as structural polymers, microtubules are dynamically regulated by a diverse repertoire of post-translational modifications (PTMs), collectively referred to as the tubulin code, which modulates microtubule stability, motor protein recruitment, cargo transport, and neuronal function (Janke and Magiera, 2020). Among these PTMs, acetylation, detyrosination, Δ2-tubulin formation, and polyglutamylation have emerged as critical regulators of axonal transport by modifying the interaction between microtubules and molecular motors. Dysregulation of the tubulin code has been increasingly implicated in neurodegenerative disorders, highlighting its importance for maintaining neuronal homeostasis. In

particular, polyglutamylation has been recognized as a key determinant of kinesin and dynein processivity, cargo selection, and the activity of microtubule-severing enzymes, thereby acting as a molecular regulator of intracellular trafficking rather than simply altering microtubule stability (Janke and Magiera, 2020; Bodakuntla et al., 2019).

Previous work from our group identified Δ2-tubulin accumulation as a pathogenic mechanism in bortezomib-induced peripheral neuropathy, demonstrating that this tubulin PTM is both necessary and sufficient to induce axonal degeneration and impair mitochondrial motility in vitro, in vivo, and in human samples (Pero et al., 2021; Iseppon et al., 2026). These findings established a direct mechanistic link between tubulin PTM dysregulation, altered organelle trafficking, and neuronal injury. They also indicate that tubulin PTM changes can act upstream of mitochondrial transport defects in at least one chemotherapeutic context. Among tubulin PTMs, polyglutamylation has emerged as a key regulator of motor protein processivity and cargo trafficking (Janke and Magiera, 2020; Bodakuntla et al., 2019). More recently, cisplatin has been shown to alter tubulin polyglutamylation and broader tubulin-code patterns in cisplatin-resistant tumor cells, reinforcing the idea that platinum exposure can remodel the tubulin code in non-neuronal systems (Horibata et al., 2026). However, the contribution of tubulin polyglutamylation to CIPN and its relationship to mitochondrial dysfunction in sensory neurons remain largely unexplored. The relative positioning of mitochondrial dysfunction and tubulin PTM remodeling during platinum-based neurotoxicity therefore remains an open question.

Building on this evidence, we asked how platinum-based compounds position mitochondrial dysfunction relative to remodeling of the tubulin PTM code in sensory neurons. Moreover, it remains unclear whether mitochondrial dysfunction alone is sufficient to drive the downstream cellular changes that culminate in axonal degeneration or whether additional mechanisms distinguish neurotoxic from non-neurotoxic chemotherapeutic agents. Addressing this question requires a comparative experimental approach capable of separating cellular responses common to chemotherapeutic exposure from those specifically associated with peripheral neurotoxicity. To address these questions, we compared Oxa, a platinum-based chemotherapeutic agent strongly associated with sensory neuropathy, with 5-fluorouracil (5-FU), an antimetabolite that is frequently co-administered in colorectal cancer treatment but is only rarely associated with clinically significant peripheral neurotoxicity. Using complementary in vivo and in vitro models, we investigated oxidative stress, mitochondrial bioenergetics, tubulin post-translational modifications (PTMs), intracellular organelle trafficking, and axonal degeneration in sensory neurons. By directly comparing a neurotoxic and a non-neurotoxic chemotherapeutic agent, we sought to distinguish cellular responses common to chemotherapeutic exposure from those specifically associated with peripheral neurotoxicity.

Our findings demonstrate that although both Oxa and 5-FU induce early mitochondrial bioenergetic dysfunction in primary sensory neurons, only Oxa elicits oxidative stress in sensory ganglia in vivo, selective polyglutamylated tubulin accumulation in vitro and in vivo, and progressive remodeling of mitochondrial and lysosomal trafficking that precedes sensory axon degeneration in primary neurons. Together, these findings identify selective loss of terminal oxidative phosphorylation, organelle trafficking and tubulin code remodeling as key cellular events that distinguish the neurotoxic response to Oxa from the more general bioenergetic stress induced by chemotherapy, providing a new framework into the mechanisms underlying platinum-induced peripheral neuropathy.

RESULTS

Oxaliplatin, but not 5-fluorouracil, induces a progressive sensory neuropathy in vivo.

To compare the neurotoxic potential of oxaliplatin (Oxa) and 5-fluorouracil (5-FU), rats were treated according to clinically relevant dosing schedules and monitored throughout treatment using

behavioral, electrophysiological, and histological assessments (Figure 1 A-H). Oxa induced a progressive sensory neuropathy characterized by cold hypersensitivity, sensory nerve dysfunction, and loss of distal sensory fibers, whereas 5-FU failed to produce detectable neuropathic alterations.
Behavioral analyses showed that mechanical sensitivity, assessed using the dynamic plantar test, remained unchanged throughout the treatment period in all experimental groups (Figure 1 A). In contrast, Oxa-treated animals developed a significant increase in nocifensive responses in the cold plate test at the experimental endpoint, indicative of cold hypersensitivity (Figure 1 B). No significant alterations in either mechanical or cold sensitivity were detected following 5-FU treatment.
Electrophysiological recordings performed at the midpoint and end of treatment further demonstrated sensory nerve dysfunction following chronic Oxa exposure.
Oxaliplatin-treated animals exhibited a significant reduction in sensory nerve action potential (SAP) amplitude in both the caudal (Figure 1C) and digital (Figure 1D) nerves at the end of treatment. Sensory nerve conduction velocity remained largely preserved, although a modest but statistically significant reduction was observed in the digital nerve during the intermediate treatment phase (Figure 1F). No significant changes in conduction velocity were detected in the caudal nerve (Figure 1E) or in either nerve at the end of treatment.
In agreement with the behavioral findings, no electrophysiological abnormalities were observed in 5-FU-treated animals. Histological analysis further supported the selective neurotoxicity of Oxa. Quantification of intraepidermal nerve fibers (IENFs) revealed a marked reduction in epidermal innervation at the experimental endpoint, consistent with the development of a length-dependent sensory axonopathy (Figure 1 G-H). In contrast, IENF density remained unchanged following 5-FU treatment. Together, these findings demonstrate that Oxa, but not 5-FU, induces a progressive sensory neuropathy characterized by cold hypersensitivity, sensory axonal dysfunction, and distal sensory fiber loss. The absence of behavioral, electrophysiological, and structural abnormalities following 5-FU treatment established these two compounds as suitable comparative models to investigate the cellular and molecular events that distinguish neurotoxic from non-neurotoxic chemotherapeutic agents. We therefore next examined whether the differential neuropathic phenotype was associated with distinct alterations in oxidative stress and mitochondrial homeostasis.

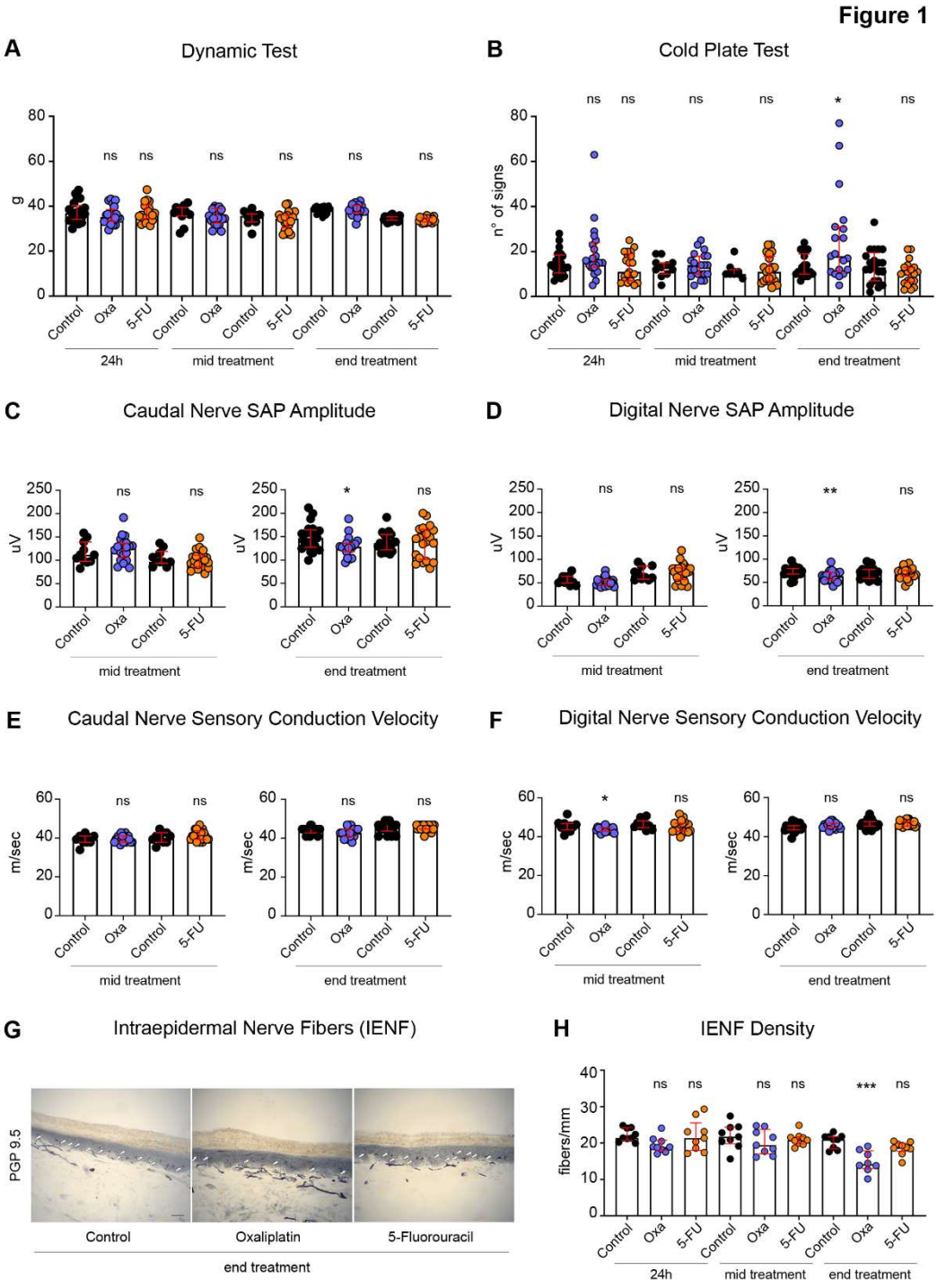


Figure 1. Oxaliplatin induces sensory alterations and reduces distal axonal integrity, with limited effects on sensory conduction velocity.

(A) Mechanical sensitivity was assessed using the dynamic plantar test at 24 h, mid-treatment, and the experimental endpoint. No significant differences were detected following oxaliplatin (OXA) or 5-fluorouracil (5-FU) treatment at any time point. At 24 h, the Kruskal-Wallis test revealed no significant differences among groups ($H(2) = 1.828$, $p = 0.4010$; Dunn's multiple-comparisons test: control vs. OXA, adjusted $p = 0.3782$; control vs. 5-FU, adjusted $p > 0.9999$). No significant differences were observed at mid-treatment (Mann–Whitney U test: OXA, $p = 0.2344$; 5-FU, $p =$

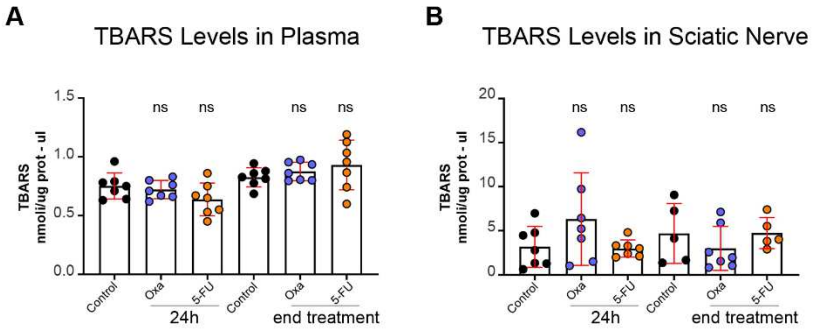
0.3429) or at the experimental endpoint (OXA, p = 0.7788; 5-FU, p = 0.0793). **(B)** Cold sensitivity was assessed using the cold plate test by quantifying nocifensive responses at 24 h, mid-treatment, and the experimental endpoint. No significant differences were observed at 24 h (Kruskal-Wallis test: H(2) = 3.603, p = 0.1651; Dunn's multiple-comparisons test: control vs. OXA, adjusted p = 0.5723; control vs. 5-FU, adjusted p = 0.8172) or at mid-treatment (Mann-Whitney U test: OXA, p = 0.8831; 5-FU, p = 0.7964). At the experimental endpoint, OXA-treated animals exhibited significantly more cold-evoked nocifensive responses than controls (Mann-Whitney U test, p = 0.0324), whereas no significant difference was detected following 5-FU treatment (p = 0.1079). **(C, D)** Sensory nerve action potential (SNAP) amplitudes were recorded from the caudal (C) and digital (D) nerves at mid-treatment and the experimental endpoint. At mid-treatment, caudal SNAP amplitudes did not differ significantly following OXA (Mann-Whitney U test, p = 0.2890) or 5-FU treatment (p = 0.6625). Similarly, digital SNAP amplitudes were not significantly altered following OXA (p = 0.2381) or 5-FU treatment (p = 0.7872). At the experimental endpoint, OXA treatment significantly reduced SNAP amplitudes in both the caudal (p = 0.0234) and digital nerves (p = 0.0083), whereas no significant changes were observed following 5-FU treatment (caudal nerve, p = 0.7652; digital nerve, p = 0.9801). **(E, F)** Sensory nerve conduction velocities were measured in the caudal (E) and digital (F) nerves at mid-treatment and the experimental endpoint. At mid-treatment, caudal nerve conduction velocity was not significantly altered following OXA (Mann-Whitney U test, p = 0.7410) or 5-FU treatment (p = 0.3409). In contrast, OXA-treated animals exhibited a modest but statistically significant reduction in digital nerve conduction velocity compared with controls (p = 0.0399), whereas no significant difference was detected following 5-FU treatment (p = 0.1892). At the experimental endpoint, neither OXA nor 5-FU significantly affected caudal nerve conduction velocity (p = 0.1003 and p = 0.7912, respectively) or digital nerve conduction velocity (p = 0.0715 and p = 0.8076, respectively).**(G)** Representative PGP9.5-immunolabeled skin sections showing intraepidermal nerve fibers (IENFs) at the experimental endpoint in control, OXA-treated, and 5-FU-treated animals. Scale bar, 500 μm.**(H)** IENF density (fibers/mm) was quantified at 24 h, mid-treatment, and the experimental endpoint. At 24 h, no significant overall difference in IENF density was detected among experimental groups (Kruskal-Wallis test, H(2) = 5.449, p = 0.0656). Although Dunn's post hoc comparison between control and OXA-treated animals yielded an adjusted p-value of 0.0427, this comparison was not interpreted as statistically significant because the overall Kruskal-Wallis test did not reach significance. No significant differences were detected at mid-treatment (Kruska-Wallis test, H(2) = 1.019, p = 0.6007). At the experimental endpoint, a significant overall difference was observed (Kruskal-Wallis test, H(2) = 12.93, p = 0.0016), with a significant reduction in IENF density in OXA-treated animals compared with controls (Dunn's multiple-comparisons test, adjusted p = 0.0007), whereas no significant difference was detected following 5-FU treatment (adjusted p = 0.2782). Data are presented as mean ± standard deviation (SD), with individual data points representing individual animals (independent biological replicates). Statistical analyses were performed using the Kruskal-Wallis test followed by Dunn's multiple-comparisons test or the two-tailed Mann-Whitney U test, as appropriate. Post hoc comparisons following the Kruskal-Wallis test were interpreted as statistically significant only when the overall test reached significance ($p < 0.05$). Exact p-values are reported in the figure legend. Statistical significance is indicated in the graphs as follows: *$p < 0.05$, **$p < 0.01$, ***$p < 0.001$; ns, not significant.

Oxaliplatin induces localized oxidative stress, selective impairment of terminal oxidative phosphorylation, and polyglutamylated tubulin accumulation during neuropathy development.

Mitochondrial dysfunction and cytoskeletal alterations have both been implicated in the pathogenesis of chemotherapy-induced peripheral neuropathy (CIPN). To determine whether these processes develop during Oxa-induced neuropathy, we evaluated oxidative stress, mitochondrial homeostasis, antioxidant defenses, and tubulin post-translational modifications (PTMs) in dorsal root ganglia

(DRG) and sciatic nerves collected from rats treated with Oxa or 5-FU. Oxidative stress was first assessed by measuring thiobarbituric acid reactive substances (TBARS), an indicator of lipid peroxidation and reactive oxygen species (ROS) production. We found that Oxa treatment induced a significant increase in TBARS levels in DRG tissue at both mid-treatment and the experimental endpoint, whereas no changes were observed following 5-FU administration (Figure 2 A). Importantly, this increase was restricted to sensory ganglia, as TBARS levels remained unchanged in plasma and sciatic nerve throughout treatment (Figure 1 S A-B), indicating that oxidative stress develops locally within sensory neurons rather than reflecting a generalized systemic response to chemotherapy. To determine whether increased oxidative stress was accompanied by alterations in endogenous antioxidant defenses, we quantified the expression of key antioxidant enzymes involved in ROS detoxification. At mid-treatment, Oxa induced a modest increase in catalase (CAT) expression, consistent with an early adaptive response (Figure 2 B). Following chronic treatment, however, the expression of SOD1, SOD2, CAT, and GSR was significantly reduced, indicating progressive impairment of antioxidant defenses and disruption of redox homeostasis. In contrast, no significant alterations in antioxidant gene expression were detected following 5-FU treatment. Because mitochondria are both a major source and target of ROS, we next examined mitochondrial homeostasis in DRG tissue. Immunoblot analysis of oxidative phosphorylation (OXPHOS) proteins revealed a selective reduction in the Complex IV subunit mt-COX2 and the ATP synthase subunit ATP5A1 at both mid- and end-treatment, whereas NDUFB8 (Complex I), SDHB (Complex II), and UQCRC2 (Complex III) remained largely unchanged (Figure 2 C-D). This profile argues against a generalized loss of mitochondrial content and instead suggests selective remodeling of terminal oxidative phosphorylation and ATP-generating machinery. Because Complex IV and ATP synthase are essential for maintaining mitochondrial membrane potential and ATP production, these findings are consistent with the development of mitochondrial dysfunction during Oxa-induced neuropathy. Notably, reductions in mt-COX2 and ATP5A1 preceded the most pronounced behavioral and structural manifestations of neuropathy, suggesting that mitochondrial remodeling occurs early during disease progression. Microtubules and their associated post-translational modifications (PTMs) are critical regulators of intracellular trafficking and neuronal homeostasis. We therefore investigated whether Oxa-induced neuropathy was associated with alterations in the tubulin PTM code. Among the PTMs examined, we found that polyglutamylated tubulin (polyE) was the only modification significantly altered in vivo. Immunofluorescence analysis revealed a progressive increase in polyE levels in both DRG neuronal cell bodies and sciatic nerve axons during Oxa treatment (Figure 2 E-F). In DRG, polyE accumulation became apparent at mid-treatment and remained elevated at the experimental endpoint, whereas sciatic nerves exhibited a progressive increase over time. In contrast, 5-FU treatment did not alter polyE levels in either DRG or sciatic nerve (Figure 2 G-H). To determine whether Oxa selectively affected polyglutamylation or induced broader remodeling of the tubulin PTM code, we also examined acetylated, detyrosinated, and Δ2-tubulin in DRG and sciatic nerve. In contrast to polyglutamylation, acetylated, detyrosinated, and Δ2-tubulin remained unchanged following Oxa treatment in both tissues (Figure 2 S A-B), and 5-FU similarly failed to alter any of the tubulin PTMs analyzed (Figure 2 S C-D), indicating that polyglutamylation is the predominant tubulin PTM associated with Oxa-induced peripheral neuropathy. Collectively, these findings demonstrate that chronic Oxa in vivo treatment, but not 5-FU, induces localized oxidative stress in sensory ganglia, impairs antioxidant defenses, selectively remodels terminal oxidative phosphorylation, and promotes the accumulation of polyglutamylated tubulin during neuropathy development. These in vivo observations prompted us to investigate whether the differential neurotoxicity of Oxa and 5-FU could be explained by distinct effects on mitochondrial function and tubulin remodeling in primary sensory neurons.

Figure 1S



Supplementary Figure S1. Plasma and sciatic nerve TBARS levels following oxaliplatin and 5-fluorouracil treatment.

(A) Thiobarbituric acid-reactive substances (TBARS) levels measured in plasma isolated from blood samples collected from control, oxaliplatin (OXA)-treated, and 5-fluorouracil (5-FU)-treated animals at 24 h and at the experimental endpoint. No significant differences were detected among groups at 24 h (Kruskal-Wallis test, $H(2) = 2.506$, $p = 0.2954$; $n = 7$ animals per group) or at the experimental endpoint ($H(2) = 1.900$, $p = 0.4024$; $n = 7$ animals per group). Dunn's multiple-comparisons test revealed no significant differences between control and OXA (24 h, adjusted $p > 0.9999$; endpoint, adjusted $p = 0.9814$) or between control and 5-FU (24 h, adjusted $p = 0.2853$; endpoint, adjusted $p = 0.3362$). **(B)** TBARS levels measured in sciatic nerve tissue collected from control, OXA-treated, and 5-FU-treated animals at 24 h and at the experimental endpoint. No significant differences were detected among groups at 24 h (Kruskal-Wallis test, $H(2) = 2.056$, $p = 0.3717$; $n = 7$ animals per group) or at the experimental endpoint ($H(2) = 2.501$, $p = 0.3033$; control, $n = 5$; OXA, $n = 7$; 5-FU, $n = 5$). Dunn's multiple-comparisons test revealed no significant differences between control and OXA (24 h, adjusted $p = 0.3636$; endpoint, adjusted $p = 0.4769$) or between control and 5-FU (24 h, adjusted $p > 0.9999$; endpoint, adjusted $p > 0.9999$). Data are presented as mean ± standard deviation (SD), with each data point representing one animal (biological replicate). Statistical significance was defined as $p < 0.05$; ns indicates not significant.

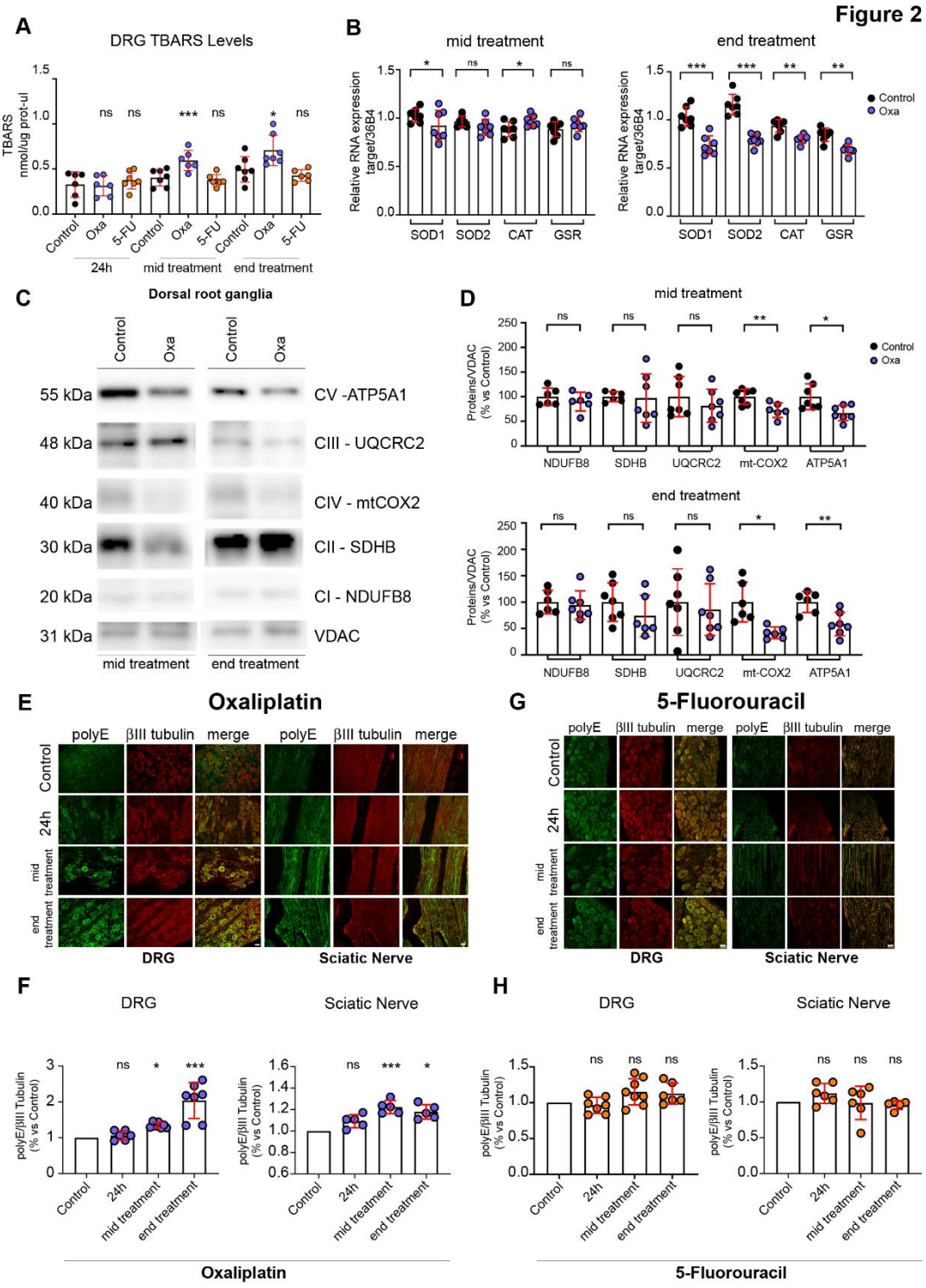
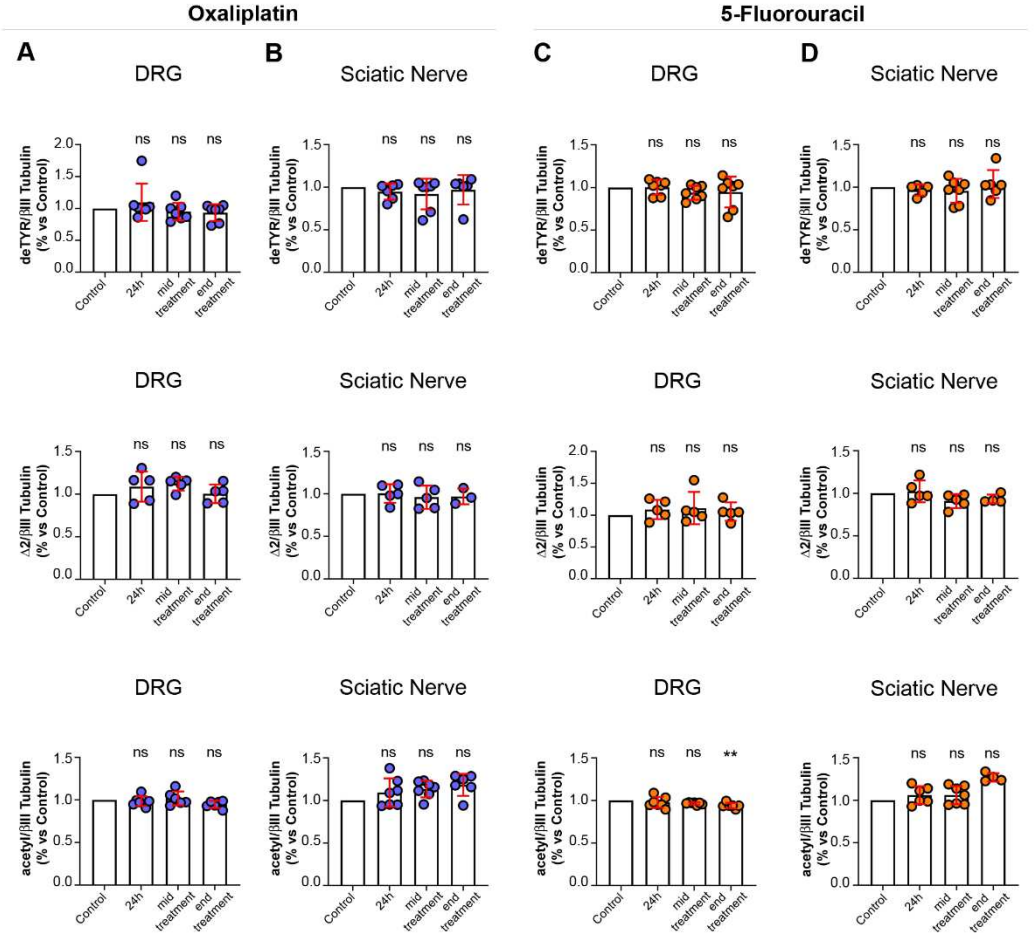


Figure 2. Oxaliplatin induces oxidative stress, impairs mitochondrial homeostasis, and increases tubulin polyglutamylation in sensory neurons during neuropathy development.
(A) Lipid peroxidation was assessed by measuring thiobarbituric acid-reactive substances (TBARS) in dorsal root ganglia (DRG) from control rats and rats treated with oxaliplatin (Oxa) or 5-fluorouracil (5-FU) at three experimental time points: 24 h, mid-treatment, and end-treatment. Data are presented as mean ± standard deviation (SD), with individual data points representing independent biological replicates (one animal per data point). Sample sizes were as follows: 24 h, control n = 6, Oxa n = 6, and 5-FU n = 7; mid-treatment, control n = 7, Oxa n = 6, and 5-FU n = 7; end-treatment, control n = 7, Oxa n = 7, and 5-FU n = 6. Statistical analyses were performed independently at each time point

using ordinary one-way ANOVA followed by Dunnett's multiple-comparisons test against the corresponding control group. At 24 h, no significant differences were detected among groups ($F(2,16) = 0.5059$, $p = 0.6123$; Oxa vs. control, adjusted $p = 0.9676$; 5-FU vs. control, adjusted $p = 0.6888$). At mid-treatment, a significant overall difference was observed ($F(2,17) = 11.01$, $p = 0.0009$), with increased TBARS levels in Oxa-treated animals (adjusted $p = 0.0027$), whereas 5-FU had no significant effect (adjusted $p = 0.7839$). At end-treatment, ANOVA also revealed a significant difference among groups ($F(2,17) = 7.627$, $p = 0.0043$). TBARS levels were significantly elevated in Oxa-treated animals (adjusted $p = 0.0183$), but not in the 5-FU group (adjusted $p = 0.5885$). Normality of residuals and homogeneity of variances were assessed using the Shapiro-Wilk and Brown-Forsythe tests, respectively, with no statistically significant violations detected. **(B)** Relative expression of antioxidant defense-related genes, including superoxide dismutase 1 (SOD1), superoxide dismutase 2 (SOD2), catalase (CAT), and glutathione-disulfide reductase (GSR), in DRG from control and Oxa-treated rats at mid-treatment and end-treatment. Each data point represents an independent biological replicate (one animal). Comparisons between control and Oxa groups were performed separately for each gene and time point using exact, two-tailed Mann-Whitney U tests. At mid-treatment, significant differences were detected for SOD1 (control $n = 7$, Oxa $n = 6$; $U = 5$, $p = 0.0221$) and CAT (control $n = 7$, Oxa $n = 7$; $U = 8.5$, $p = 0.0396$), whereas SOD2 (control $n = 7$, Oxa $n = 7$; $U = 11.5$, $p = 0.1008$) and GSR (control $n = 7$, Oxa $n = 7$; $U = 17$, $p = 0.3625$) did not differ significantly between groups. At end-treatment, significantly reduced expression was observed for all four genes: SOD1 (control $n = 7$, Oxa $n = 7$; $U = 0$, $p = 0.0006$), SOD2 (control $n = 7$, Oxa $n = 7$; $U = 0$, $p = 0.0006$), CAT (control $n = 7$, Oxa $n = 6$; $U = 2$, $p = 0.0041$), and GSR (control $n = 7$, Oxa $n = 7$; $U = 1.5$, $p = 0.0017$). Statistical significance was assessed using unadjusted p-values. **(C)** Representative Western blots showing the expression of mitochondrial oxidative phosphorylation (OXPHOS) proteins in DRG from control and Oxa-treated rats at mid-treatment and end-treatment. The analyzed proteins included NDUFB8 (complex I), SDHB (complex II), UQCRC2 (complex III), mitochondrially encoded cytochrome c oxidase II (mt-COX2; complex IV), and ATP synthase subunit alpha (ATP5A1; complex V). Voltage-dependent anion channel (VDAC) was used as the loading control. **(D)** Densitometric quantification of mitochondrial OXPHOS proteins shown in panel C. Protein levels were normalized to VDAC and expressed as a percentage of the corresponding control group, set to 100%. Data are presented as mean ± SD, with individual data points representing independent biological replicates (one animal per data point). Comparisons between control and Oxa-treated groups were performed independently for each protein and treatment time point using two-tailed unpaired Welch's t-tests. At mid-treatment, no statistically significant differences were detected for NDUFB8 ($t = 0.9339$, $df = 9.936$, $p = 0.3725$), SDHB ($t = 0.1534$, $df = 6.591$, $p = 0.8827$), or UQCRC2 ($t = 0.9281$, $df = 11.58$, $p = 0.3723$). In contrast, mt-COX2 ($t = 3.273$, $df = 10.75$, $p = 0.0076$; control $n = 7$, Oxa $n = 6$) and ATP5A1 ($t = 2.882$, $df = 9.710$, $p = 0.0168$; control $n = 7$, Oxa $n = 7$) were significantly reduced. At end-treatment, no statistically significant differences were observed for NDUFB8 ($t = 0.4152$, $df = 10.00$, $p = 0.6860$), SDHB ($t = 1.235$, $df = 10.40$, $p = 0.2441$), or UQCRC2 ($t = 0.4696$, $p = 0.6475$). Conversely, mt-COX2 expression was reduced by 58.15% ($t = 3.624$, $p = 0.0115$; control $n = 6$, Oxa $n = 6$), and ATP5A1 expression was reduced by 41.50% ($t = 3.580$, $p = 0.0043$; control $n = 6$, Oxa $n = 7$), compared with controls. **(E, G)** Representative immunofluorescence images of DRG and sciatic nerve sections from control rats and animals treated with Oxa (E) or 5-FU (G) at 24 h, mid-treatment, and end-treatment. Sections were immunostained for polyglutamylated tubulin (polyE, green) and βIII-tubulin (red). Merged images are shown. Scale bars, 100 μm. **(F)** Quantification of tubulin polyglutamylation in DRG and sciatic nerves from control and Oxa-treated rats at 24 h, mid-treatment, and end-treatment. PolyE immunofluorescence intensity was normalized to βIII-tubulin immunofluorescence intensity and expressed relative to controls. In DRG, the Kruskal-Wallis test revealed significant differences among groups ($H(3) = 20.79$, $p = 0.0001$). Dunn's multiple-comparisons test showed significantly increased polyglutamylation at mid-treatment (adjusted $p = 0.0435$) and end-treatment (adjusted $p = 0.0005$), but not at 24 h (adjusted $p > 0.9999$), compared with controls (control $n = 6$; 24 h $n = 6$; mid-treatment $n = 7$; end-treatment $n =$

7). Similarly, significant differences were detected among groups in sciatic nerves (Kruskal-Wallis, H(3) = 14.94, p = 0.0019). Dunn's multiple-comparisons test revealed increased polyglutamylation at mid-treatment (adjusted p = 0.0009) and end-treatment (adjusted p = 0.0129), whereas no significant difference was observed at 24 h (adjusted p = 0.3180; n = 5 per group). **(H)** Quantification of tubulin polyglutamylation in DRG and sciatic nerves from control and 5-FU-treated rats at the same experimental time points, performed as described for panel F. In DRG, no statistically significant differences were detected among groups (Kruskal-Wallis, H(3) = 7.486, p = 0.0579). Dunn's multiple-comparisons test showed no significant differences at 24 h (adjusted p > 0.9999), mid-treatment (adjusted p = 0.3717), or end-treatment (adjusted p = 0.4263), compared with controls (control n = 7; 24 h n = 7; mid-treatment n = 8; end-treatment n = 6). Likewise, sciatic nerve polyglutamylation did not differ significantly among groups (Kruskal-Wallis, H(3) = 5.697, p = 0.1273). No significant differences were observed at 24 h (adjusted p = 0.5084), mid-treatment (adjusted p > 0.9999), or end-treatment (adjusted p = 0.8726), compared with controls (control n = 6; 24 h n = 6; mid-treatment n = 6; end-treatment n = 5). For panels F and H, statistical analyses were performed using the Kruskal-Wallis test followed by Dunn's multiple-comparisons test. Adjusted p-values are reported for comparisons with the corresponding control group. Individual data points represent independent biological replicates (one animal per data point). *Statistical significance:* *p < 0.05, **p < 0.01, ***p < 0.001; ns, not significant. Significance thresholds refer to adjusted p-values for panels A, F, and H and to unadjusted p-values for panels B and D.

Figure 2S



Supplementary Figure S2. Effects of oxaliplatin and 5-fluorouracil on tubulin post-translational modifications in dorsal root ganglia and sciatic nerves.
(A, B) Quantification of detyrosinated (deTyr), Δ2-, and acetylated α-tubulin in dorsal root ganglia (DRG; A) and sciatic nerves (B) from control and oxaliplatin-treated (OXA) rats at 24 h, mid-

treatment, and end-treatment. Immunofluorescence intensities were normalized to βIII-tubulin fluorescence intensity and expressed relative to the corresponding control group, set to 1. (A) In DRG, no significant overall differences in detyrosinated tubulin levels were detected among groups (ordinary one-way ANOVA, $F(3,23) = 1.180$, $p = 0.3390$). Dunnett's multiple-comparisons test confirmed no significant differences at 24 h (adjusted $p = 0.6304$), mid-treatment (adjusted $p = 0.9232$), or end-treatment (adjusted $p = 0.8477$). Similarly, Δ2-tubulin levels did not differ significantly among experimental groups at the examined time points. Acetylated tubulin levels showed no significant overall differences (Kruskal-Wallis test, $H(3) = 7.811$, $p = 0.0501$). Although Dunn's multiple-comparisons test yielded an adjusted p-value of 0.0217 for the comparison between control and end-treatment groups, this comparison was not interpreted as statistically significant because the overall Kruskal-Wallis test did not reach significance. No significant differences were observed at 24 h (adjusted $p = 0.2857$) or mid-treatment (adjusted $p > 0.9999$). (B) In sciatic nerves, no significant overall differences in Δ2-tubulin levels were detected among groups (Kruskal-Wallis test, $H(3) = 0.9467$, $p = 0.8402$). Dunn's multiple-comparisons test confirmed no significant differences at 24 h, mid-treatment, or end-treatment (adjusted $p > 0.9999$ for all comparisons). Similarly, detyrosinated and acetylated tubulin levels did not show significant differences at any of the examined time points. **(C, D)** Quantification of detyrosinated, Δ2-, and acetylated α-tubulin in DRG (C) and sciatic nerves (D) from control and 5-fluorouracil-treated (5-FU) rats at 24 h, mid-treatment, and end-treatment. Immunofluorescence intensities were normalized to βIII-tubulin fluorescence intensity and expressed relative to the corresponding control group, set to 1. (C) In DRG, detyrosinated tubulin levels did not differ significantly among groups (Kruskal-Wallis test, $H(3) = 2.995$, $p = 0.3924$). Dunn's multiple-comparisons test revealed no significant differences at 24 h (adjusted $p = 0.6049$), mid-treatment (adjusted $p > 0.9999$), or end-treatment (adjusted $p > 0.9999$). Similarly, no significant overall differences in Δ2-tubulin levels were detected (Kruskal-Wallis test, $H(3) = 2.570$, $p = 0.4628$). Dunn's multiple-comparisons test confirmed no significant differences at 24 h (adjusted $p = 0.3946$), mid-treatment (adjusted $p = 0.8442$), or end-treatment (adjusted $p = 0.7082$). In contrast, acetylated tubulin levels differed significantly among groups (Kruskal–Wallis test, $H(3) = 11.87$, $p = 0.0078$). Dunn's multiple-comparisons test revealed a significant reduction in acetylated tubulin levels at end-treatment (adjusted $p = 0.0019$), whereas no significant differences were detected at 24 h (adjusted $p = 0.1970$) or mid-treatment (adjusted $p = 0.0959$). (D) In sciatic nerves from 5-FU-treated rats, no statistically significant differences in detyrosinated, Δ2-, or acetylated tubulin levels were detected at any of the examined time points compared with controls. Data are presented as mean ± standard deviation (SD), with individual data points representing individual animals (independent biological replicates). Sample sizes (n) refer to the number of animals analyzed per experimental group. Statistical analyses were performed using ordinary one-way ANOVA followed by Dunnett's multiple-comparisons test or the Kruskal-Wallis test followed by Dunn's multiple-comparisons test, as appropriate. Statistical comparisons were performed against the corresponding control group, and adjusted p-values are reported. Post hoc comparisons following the Kruskal-Wallis test were interpreted as statistically significant only when the overall test reached significance ($p < 0.05$). Statistical significance: $*p < 0.05$, $**p < 0.01$, $***p < 0.001$; ns, not significant.

Primary DRG cultures reproduce the differential neurotoxic effects of oxaliplatin and 5-fluorouracil observed in vivo

To determine whether the differential neurotoxicity observed in vivo could be recapitulated in an isolated neuronal system, primary adult dorsal root ganglion (DRG) neurons (5 DIV) were exposed to increasing physiologically relevant concentrations of Oxa or 5-FU, and neurite integrity was evaluated by neurofilament immunostaining (Figure 3 A-C). Dose response analysis performed 72 h after treatment revealed a concentration-dependent increase in neurite degeneration following Oxa

exposure, with significant increases in both degeneration index and retraction bulb formation at 5 nM and 10 nM compared with control cultures (Figure 3 D-E). In contrast, 5-FU did not significantly affect neurite morphology or degeneration index over the concentration range tested, although a modest increase in retraction bulbs was observed at the highest concentration (750 nM) (Figure 3 D-E). Time-course analysis further demonstrated that Oxa-induced neurite degeneration developed progressively. Representative neurofilament-stained cultures showed preserved neurite architecture at 12 and 24 h, followed by extensive fragmentation and neurite loss after 48 h of Oxa (10 nM) treatment (Figure 3 B). Quantitative analysis confirmed a significant increase in degeneration index only at the 48-h time point (Figure 3 F). By contrast, neurite morphology remained largely preserved throughout the entire experimental period following 5-FU(500 nM) treatment, with no significant changes in degeneration index detected at 12, 24, or 48 h (Figure 3 C and G). Collectively, these findings indicate that primary adult DRG cultures faithfully reproduce the differential neurotoxic profile observed in vivo, with Oxa inducing progressive neurite degeneration whereas 5-FU causing only minimal structural changes. This in vitro system therefore provides a suitable experimental platform to dissect the cellular mechanisms underlying the distinct neurotoxic properties of these two chemotherapeutic agents.

Figure 3

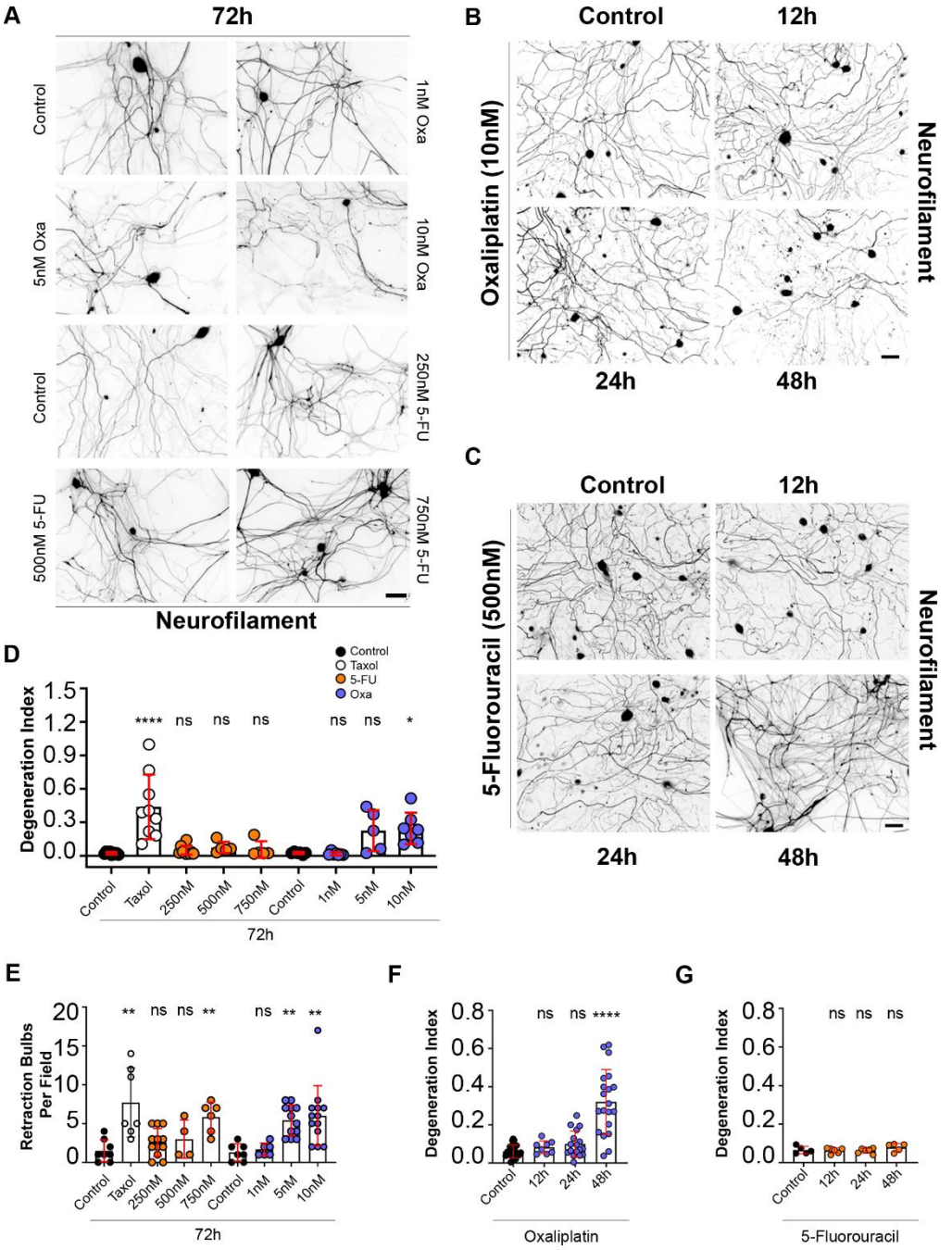


Figure 3. Oxaliplatin induces neurite degeneration in primary DRG neurons, whereas 5-fluorouracil shows limited structural effects.

(A) Representative images of neurofilament-stained primary dorsal root ganglion (DRG) neurons following 72 h of exposure to increasing concentrations of oxaliplatin (OXA; 1, 5, and 10 nM) or 5-fluorouracil (5-FU; 250, 500, and 750 nM), compared with untreated controls. Scale bars, 100 µm.

(B, C) Representative neurofilament-stained images showing time-dependent changes in neurite morphology following exposure to OXA (10 nM; B) or 5-FU (500 nM; C) for 12, 24, and 48 h. OXA treatment was associated with progressive structural alterations, whereas comparatively limited changes were observed following 5-FU exposure. **(D)** Quantification of the axonal degeneration index following 72 h of exposure to increasing concentrations of OXA or 5-FU. Paclitaxel (Taxol; 50 nM) was included as a positive control for axonal degeneration. Statistical analysis was performed across all eight experimental groups using the Kruskal-Wallis test, which revealed a significant overall difference ($H(7) = 39.72$, $p < 0.0001$; 57 observations). Dunn's multiple-comparisons test showed a significant increase in the degeneration index following treatment with OXA at 10 nM (adjusted $p = 0.0029$), whereas no significant differences were detected at 1 nM (adjusted $p > 0.9999$) or 5 nM (adjusted $p = 0.0567$). No significant differences were observed following 5-FU treatment at 250 nM (adjusted $p > 0.9999$), 500 nM (adjusted $p = 0.4974$), or 750 nM (adjusted $p > 0.9999$). As expected, Taxol significantly increased the degeneration index compared with untreated controls (adjusted $p < 0.0001$). All seven post hoc comparisons were performed against the untreated control group. **(E)** Quantification of axonal retraction bulbs per field following 72 h of exposure to increasing concentrations of OXA or 5-FU. Paclitaxel (Taxol; 50 nM) was included as a positive control for retraction bulb formation. OXA significantly increased retraction bulb formation at 5 nM (Dunn's multiple-comparisons test, adjusted $p = 0.0013$) and 10 nM (adjusted $p = 0.0021$), but not at 1 nM. Similarly, 5-FU significantly increased retraction bulb formation at 750 nM (adjusted $p = 0.0067$), whereas no significant differences were observed at 250 or 500 nM. Taxol significantly increased retraction bulb formation compared with untreated controls (adjusted $p = 0.0028$). The previously reported Kruskal-Wallis analyses showed significant overall differences for the OXA groups ($H(3) = 21.05$, $p = 0.0001$) and the 5-FU groups including Taxol ($H(4) = 17.52$, $p = 0.0015$). **(F)** Time-dependent quantification of the axonal degeneration index in primary DRG neurons exposed to OXA (10 nM) for 12, 24, and 48 h. A significant increase in axonal degeneration was detected after 48 h of treatment (Dunn's multiple-comparisons test, adjusted $p < 0.0001$), whereas no significant differences were observed after 12 h (adjusted $p = 0.7952$) or 24 h (adjusted $p = 0.2994$). The Kruskal-Wallis test revealed a significant overall difference among groups ($H(3) = 31.76$, $p < 0.0001$). **(G)** Time-dependent quantification of the axonal degeneration index in primary DRG neurons exposed to 5-FU (500 nM) for 12, 24, and 48 h. No significant differences were detected at any time point compared with untreated controls (Kruskal-Wallis test, $H(3) = 2.164$, $p = 0.5391$; Dunn's multiple-comparisons test: adjusted $p > 0.9999$ at 12 and 24 h and adjusted $p = 0.8500$ at 48 h). Experiments were performed using primary DRG neuronal cultures from at least three independent culture preparations. All treatment conditions and time points were included in each independent experiment. For panels D-G, individual data points represent culture wells. Data are presented as mean ± standard deviation (SD), with individual experimental values displayed. Statistical analyses were performed using the Kruskal-Wallis test followed by Dunn's multiple-comparisons test against the corresponding untreated controls. Adjusted p-values are reported for pairwise comparisons. Paclitaxel (Taxol; 50 nM) served as a positive control in panels D and E. Statistical significance: *$p < 0.05$, **$p < 0.01$, ***$p < 0.001$, ****$p < 0.0001$; ns, not significant.

Oxaliplatin and 5-fluorouracil induce mitochondrial bioenergetic dysfunction in cultured adult sensory neurons

Having established that primary adult DRG cultures faithfully reproduce the differential neurotoxic effects observed in vivo, we next investigated whether mitochondrial dysfunction distinguished the response to Oxa and 5-FU. To this end, primary adult DRG neurons were exposed to either chemotherapeutic agent, and mitochondrial membrane potential and oxidative phosphorylation were evaluated in vitro (Figure 4). Mitochondrial membrane potential was first assessed using the potentiometric dye tetramethylrhodamine methyl ester (TMRM). We found that Oxa induced a progressive loss of mitochondrial membrane potential, with TMRM fluorescence remaining

unchanged at 12 h but significantly decreasing after 24 h and remaining reduced at 48 h (Figure 4 A). In contrast, 5-FU induced an earlier reduction in mitochondrial membrane potential that was already evident at 12 h and persisted throughout the experimental period (Figure 4 E), indicating that both compounds promote mitochondrial depolarization in primary sensory neurons. To determine whether mitochondrial depolarization was accompanied by impaired mitochondrial respiration, oxidative phosphorylation was evaluated using Seahorse extracellular flux analysis. We observed that Oxa treatment caused a progressive reduction in basal oxygen consumption rate (OCR), maximal respiratory capacity, and ATP-linked respiration (Figure 4 B-D). Basal respiration was significantly reduced at 24 h and declined further at 48 h. Similarly, maximal OCR and ATP-linked respiration progressively decreased over time, indicating impaired oxidative phosphorylation and reduced mitochondrial ATP-generating capacity. Unexpectedly, 5-FU produced a comparable impairment of mitochondrial respiration, with significant reductions in basal OCR, maximal respiratory capacity, and ATP-linked respiration despite the absence of overt neurite degeneration (Figure 4 F-H).

The mitochondrial bioenergetic alterations induced by Oxa closely paralleled the selective remodeling of terminal oxidative phosphorylation observed in vivo, including reduced expression of the Complex IV subunit mt-COX2 and the ATP synthase subunit ATP5A1 (Figure 2 C-D). However, the observation that both Oxa and 5-FU impaired mitochondrial membrane potential and oxidative phosphorylation, despite their markedly different neurotoxic profiles, prompted us to ask whether these agents differentially affect the tubulin PTM code, as suggested by our in vivo findings.

Figure 4

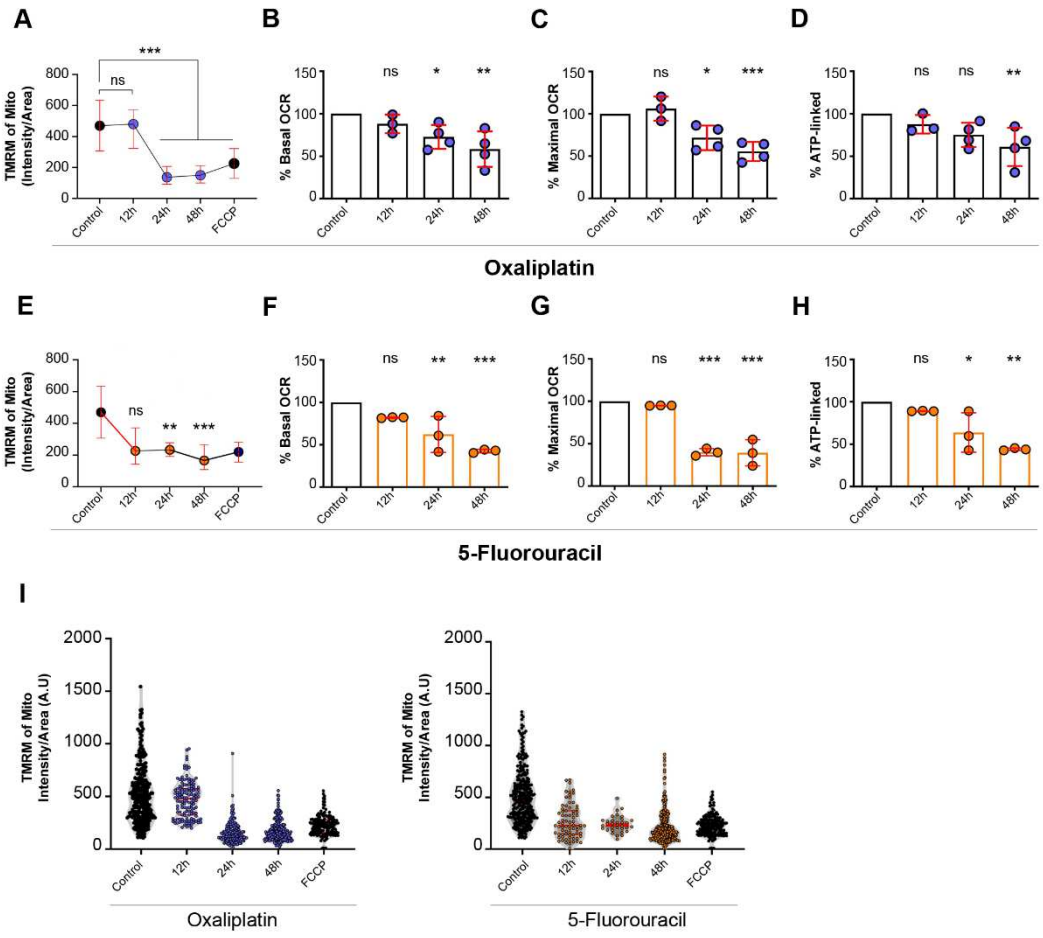


Figure 4. Oxaliplatin and 5-fluorouracil induce mitochondrial membrane depolarization and impair mitochondrial respiration in primary sensory neurons.
(A) Quantification of mitochondrial membrane potential assessed by tetramethylrhodamine methyl ester (TMRM) fluorescence in primary dorsal root ganglion (DRG) neurons following exposure to oxaliplatin (OXA; 10 nM) for 12, 24, and 48 h. Fluorescence measurements from individual mitochondria were averaged for each neurite. A total of 57 neurites were analyzed across four independent experiments. TMRM fluorescence was significantly reduced at 24 and 48 h, whereas no significant difference was observed at 12 h. Welch's one-way ANOVA revealed a significant treatment effect ($W(3, 27.19) = 41.28$, $p < 0.0001$). Dunnett's T3 multiple-comparisons test showed significant reductions at 24 and 48 h (adjusted $p < 0.0001$ for both), but not at 12 h (adjusted $p = 0.9982$). **(B–D)** Time-dependent effects of OXA (10 nM) on mitochondrial respiration in primary DRG neurons. Basal (B), maximal (C), and ATP-linked (D) oxygen consumption rates (OCR) were measured after 12, 24, and 48 h of exposure and normalized to the corresponding untreated controls (100%). Basal OCR (B) was significantly reduced at 24 h (72.79% of control; adjusted $p = 0.0475$) and 48 h (58.32%; adjusted $p = 0.0039$), but not at 12 h (adjusted $p = 0.5645$; one-way ANOVA: $F(3, 11) = 6.609$, $p = 0.0081$). Maximal OCR (C) was significantly decreased at 24 h (71.58%; adjusted $p = 0.0122$) and 48 h (55.53%; adjusted $p = 0.0005$), with no significant difference at 12 h (adjusted $p = 0.8307$; one-way ANOVA: $F(3, 11) = 16.20$, $p = 0.0002$). ATP-linked OCR (D) was significantly reduced at 48 h (60.94%; adjusted $p = 0.0085$), whereas changes at 12 h (adjusted $p = 0.5805$) and 24 h (adjusted $p = 0.0885$) were not significant (one-way ANOVA: $F(3, 11) = 5.099$, $p = 0.0188$).
(E) Quantification of mitochondrial membrane potential assessed by TMRM fluorescence in primary DRG neurons following exposure to 5-fluorouracil (5-FU; 500 nM) for 12, 24, and 48 h. Fluorescence measurements from individual mitochondria were averaged for each neurite. A total of 62 neurites were analyzed across four independent experiments. TMRM fluorescence was significantly reduced at 24 h (adjusted $p = 0.0034$) and 48 h (adjusted $p = 0.0001$), whereas no significant difference was observed at 12 h (adjusted $p = 0.0638$). FCCP, included as a positive control for mitochondrial membrane depolarization, also significantly reduced TMRM fluorescence (adjusted $p = 0.0005$). Welch's one-way ANOVA revealed a significant treatment effect ($W(4, 22.82) = 6.086$, $p = 0.0017$), followed by Dunnett's T3 multiple-comparisons test.
(F-H) Time-dependent effects of 5-FU (250 nM) on mitochondrial respiration in primary DRG neurons. Basal (F), maximal (G), and ATP-linked (H) OCR were measured after 12, 24, and 48 h of treatment and normalized to the corresponding untreated controls (100%). Basal OCR (F) was significantly reduced at 24 h (62.20% of control; adjusted $p = 0.0063$) and 48 h (42.58%; adjusted $p = 0.0004$), but not at 12 h (adjusted $p = 0.2084$; one-way ANOVA: $F(3, 8) = 16.53$, $p = 0.0009$). Maximal OCR (G) was significantly decreased at 24 h (39.97%; adjusted $p < 0.0001$) and 48 h (39.28%; adjusted $p < 0.0001$), whereas no significant difference was observed at 12 h (adjusted $p = 0.8934$; one-way ANOVA: $F(3, 8) = 52.47$, $p < 0.0001$). ATP-linked OCR (H) was significantly reduced at 24 h (63.83%; adjusted $p = 0.0132$) and 48 h (44.05%; adjusted $p = 0.0010$), but not at 12 h (adjusted $p > 0.9999$; one-way ANOVA: $F(3, 8) = 16.98$, $p = 0.0008$).
(I) Distribution of individual mitochondrial TMRM fluorescence measurements following exposure to OXA (10 nM; left) or 5-FU (500 nM; right) for 12, 24, and 48 h. Scatter plots display the fluorescence intensity measurements obtained from individual mitochondria, with each point representing a single mitochondrion. The distributions were generated from the same experimental datasets used for the neurite-level analyses presented in panels A and E. These plots are provided for descriptive purposes only. Statistical comparisons between experimental groups were performed using neurite-level measurements rather than treating individual mitochondria as independent biological replicates. TMRM measurements (A, E, I) were obtained from four independent experiments, with approximately 160 mitochondria analyzed across 10-16 neurites per experimental condition. OCR measurements (B-D, F-H) were performed using technical triplicates across 3-4 independent experiments for OXA and three independent experiments for 5-FU. TMRM data were analyzed using Welch's one-way ANOVA followed by Dunnett's T3 multiple-comparisons test,

whereas OCR data were analyzed using ordinary one-way ANOVA followed by Dunnett's multiple-comparisons test. Data in panels A-H are presented as mean ± standard deviation (SD). Adjusted p-values are reported for pairwise comparisons. Statistical significance: *p < 0.05, **p < 0.01, ***p < 0.001, ****p < 0.0001; ns, not significant.

Oxaliplatin, but not 5-fluorouracil, selectively induces polyglutamylated tubulin accumulation in primary sensory neurons

Because polyglutamylation was the only tubulin PTM altered in vivo (Figure 2 E-H), we first examined whether this modification was similarly regulated in primary adult DRG neurons. Consistent with the in vivo findings, immunoblot analysis revealed a progressive increase in polyglutamylated tubulin (polyE) following Oxa but not 5-FU treatment (Figure 5 A-B). PolyE levels remained unchanged at 12 and 24 h but increased significantly after 48 h of treatment. Thus, unlike the early bioenergetic changes observed in both Oxa and 5-FU-treated neurons, polyglutamylation developed only after prolonged Oxa exposure. To determine whether this response reflected selective polyglutamylation or a broader remodeling of the tubulin PTM code, we next examined additional tubulin PTMs.

In contrast to polyglutamylation, acetylated, detyrosinated, and Δ2-tubulin levels remained unchanged following Oxa treatment at all time points examined (Figure 3 S A-C). Likewise, 5-FU did not alter acetylated, detyrosinated, or Δ2-tubulin levels (Figure 3 S D-F), indicating that Oxa selectively increases polyglutamylation rather than inducing a generalized remodeling of the tubulin PTM landscape. Collectively, these findings identify polyglutamylation as the only tubulin PTM selectively induced by Oxa in primary sensory neurons, raising the possibility that this modification modulates microtubule-dependent organelle transport.

Figure 5

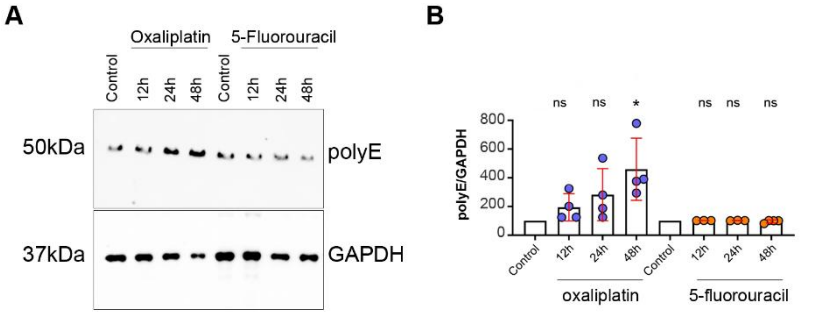
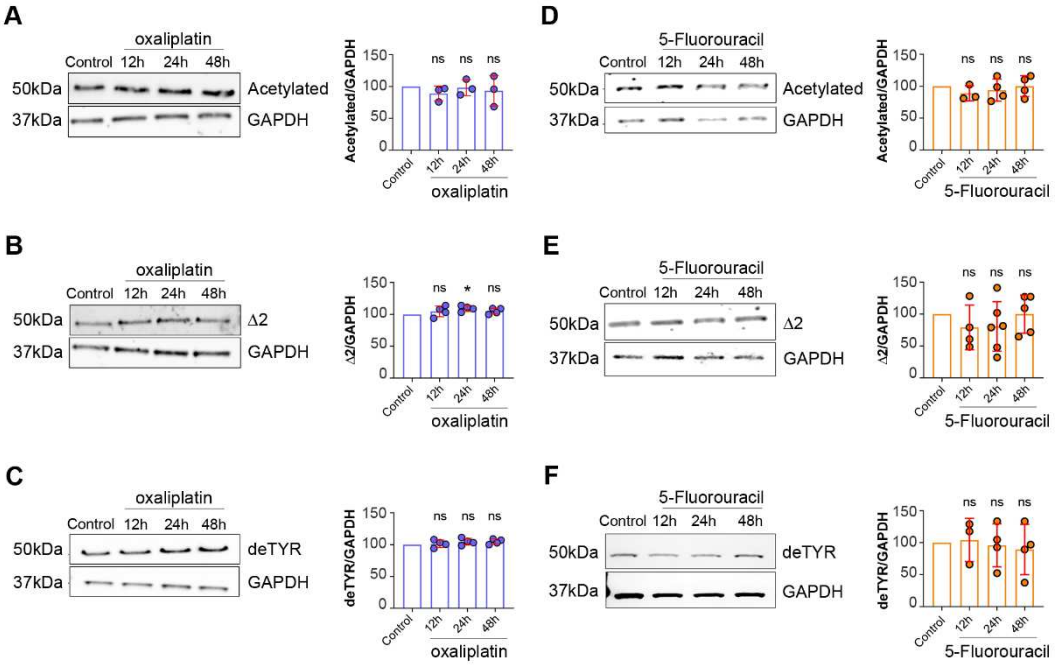


Figure 5. Oxaliplatin induces delayed accumulation of polyglutamylated tubulin in primary sensory neurons, with no comparable increase following 5-fluorouracil exposure.
(A) Representative Western blots showing polyglutamylated tubulin (polyE) levels in primary dorsal root ganglion (DRG) neurons cultured for 5 days in vitro (5 DIV) and exposed to oxaliplatin (OXA; 10 nM) or 5-fluorouracil (5-FU; 500 nM) for 12, 24, and 48 h, together with their respective untreated controls. GAPDH was used as the loading control. **(B)** Densitometric quantification of polyE immunoreactivity normalized to GAPDH and expressed as a percentage of the corresponding untreated controls (100%). Data are presented as mean ± standard deviation (SD), with individual data points representing independent biological experiments. Each experiment consisted of a primary

DRG neuronal culture preparation in which untreated controls and the corresponding treatment conditions were analyzed in parallel. For OXA-treated neurons (n = 4 independent experiments per condition), differences among treatment conditions were assessed using the Friedman test for matched observations (Friedman statistic = 8.10, exact p = 0.0329), followed by Dunn's multiple-comparisons test against untreated controls. PolyE levels were significantly increased after 48 h of OXA exposure, whereas no significant differences were detected at 12 or 24 h. For 5-FU-treated neurons (n = 3-4 independent experiments per condition), differences among treatment conditions were assessed using a mixed-effects model with restricted maximum likelihood (REML) estimation to account for matched observations and missing values. No significant overall treatment effect was detected (p = 0.4469). Dunnett's multiple-comparisons test revealed no significant differences compared with untreated controls at 12 h (adjusted p = 0.1653), 24 h (adjusted p = 0.3398), or 48 h (adjusted p = 0.7554). Statistical significance: *p < 0.05; ns, not significant.

Figure 3S



Supplementary Figure S3. Effects of oxaliplatin and 5-fluorouracil on tubulin post-translational modifications in primary adult DRG neurons.
(A-C) Representative Western blots and corresponding densitometric quantification of acetylated tubulin (A), Δ2-tubulin (B), and detyrosinated tubulin (deTyr; C) in primary adult dorsal root ganglion (DRG) neurons following exposure to oxaliplatin (OXA) for 12, 24, and 48 h. **(A)** Acetylated tubulin levels did not differ significantly among treatment conditions (Kruskal-Wallis test, H(3) = 2.626, p = 0.4997). Dunn's multiple-comparisons test revealed no significant differences relative to untreated controls at 12 h (adjusted p = 0.3312), 24 h (adjusted p > 0.9999), or 48 h (adjusted p = 0.9143). **(B)** For Δ2-tubulin, no significant overall differences were detected among treatment conditions (Kruskal-Wallis test, H(3) = 6.315, p = 0.0888). Although Dunn's multiple-comparisons test yielded an adjusted p-value of 0.0382 for the comparison between untreated controls and neurons exposed to OXA for 24 h, this comparison was not interpreted as statistically significant because the overall Kruskal-Wallis test did not reach significance. No significant differences were observed at 12 h (adjusted p = 0.4544) or 48 h (adjusted p = 0.3932). **(C)** Detyrosinated tubulin levels did not differ significantly among treatment conditions (Kruskal-Wallis test, H(3) = 3.443, p = 0.3478). Dunn's multiple-comparisons test revealed no significant differences at 12 h (adjusted p = 0.9255), 24 h (adjusted p = 0.3660), or 48 h (adjusted p = 0.2910). **(D-F)** Representative Western blots and corresponding densitometric quantification of acetylated tubulin (D), Δ2-tubulin (E), and

detyrosinated tubulin (deTyr; F) in primary adult DRG neurons following exposure to 5-fluorouracil (5-FU) for 12, 24, and 48 h. **(D)** Acetylated tubulin levels did not differ significantly among treatment conditions (Kruskal-Wallis test, $H(3) = 1.404$, $p = 0.7380$). Dunn's multiple-comparisons test revealed no significant differences at 12, 24, or 48 h (adjusted $p > 0.9999$ for all comparisons). **(E)** Δ2-tubulin levels did not differ significantly among treatment conditions (Kruskal-Wallis test, $H(3) = 1.891$, $p = 0.5953$). No significant differences were observed at 12 h (adjusted $p = 0.9827$), 24 h (adjusted $p > 0.9999$), or 48 h (adjusted $p > 0.9999$). **(F)** Detyrosinated tubulin levels did not differ significantly among treatment conditions (Kruskal-Wallis test, $H(3) = 0.9588$, $p = 0.8371$). Dunn's multiple-comparisons test revealed no significant differences at 12, 24, or 48 h (adjusted $p > 0.9999$ for all comparisons). Protein expression was normalized to GAPDH and expressed as a percentage of the corresponding untreated control group (100%). Data are presented as mean ± standard deviation (SD), with individual data points representing independent biological experiments (n = 3–6 per group). Statistical analyses were performed using the Kruskal-Wallis test followed by Dunn's multiple-comparisons test against untreated controls. Post hoc comparisons were interpreted as statistically significant only when the overall Kruskal-Wallis test reached significance ($p < 0.05$). Exact or adjusted p-values are reported in the legend. Statistical significance: $*p < 0.05$; ns, not significant.

Oxaliplatin, but not 5-fluorouracil, remodels intracellular organelle trafficking in primary sensory neurons

Given the established role of tubulin polyglutamylation in regulating microtubule-motor protein interactions, we next investigated whether the selective accumulation of polyglutamylated tubulin induced by Oxa was associated with alterations in intracellular organelle trafficking. Mitochondrial and lysosomal dynamics were therefore examined by live-cell imaging in primary adult DRG neurons following exposure to Oxa (Figures 6) or 5-FU (Figure 5S) To assess mitochondrial transport, DRG neurons expressing Mito-DsRed were imaged after 12, 24, or 48 h of Oxa treatment (Figure 6 A-B). Quantitative analysis revealed a progressive remodeling of mitochondrial dynamics. As early as 12 h, Oxa surprisingly reduced the proportion of dynamically paused mitochondria while increasing anterograde transport, indicating enhanced mitochondrial motility. At this time point, mitochondrial membrane potential and respiratory function were largely preserved (Figure 4 A), suggesting that alterations in mitochondrial trafficking precede overt bioenergetic impairment. By 24 h, the stationary mitochondrial population was significantly reduced, whereas retrograde transport remained unchanged. A significant increase in retrograde-moving mitochondria emerged only after 48 h of treatment, indicating a delayed shift in transport direction during prolonged Oxa exposure. In contrast to Oxa, 5-FU did not significantly alter mitochondrial trafficking, as the proportions of dynamically paused, stationary, anterograde and retrograde moving mitochondria remained comparable to untreated controls at all time points examined (Figure 4 S, A and B). Because mitochondrial trafficking was altered by Oxa, we next examined lysosomal dynamics using LAMP1-mCherry live-cell imaging (Figure 6 C and D). Unlike mitochondria, lysosomal transport remained largely preserved during the early stages of Oxa exposure. However, beginning at 48 h and becoming more pronounced at 72 and 96 h, lysosomes exhibited a progressive increase in stationary and dynamically paused populations together with a marked reduction in actively moving lysosomes, indicating impaired lysosomal trafficking. Lysosomal dynamics were completely preserved following 5-FU treatment, with no significant changes detected in dynamically paused, stationary, or actively moving lysosomal populations (Figure 4 S C and D). Altogether these findings demonstrate that Oxa, but not 5-FU, induces a staged remodeling of intracellular organelle trafficking characterized by an early increase in mitochondrial motility followed by delayed impairment of lysosomal transport. The preservation of both mitochondrial and lysosomal trafficking following 5-FU treatment, despite comparable mitochondrial bioenergetic dysfunction (Figure 4), indicates that altered organelle dynamics represent a selective feature of the Oxa-induced cellular response.

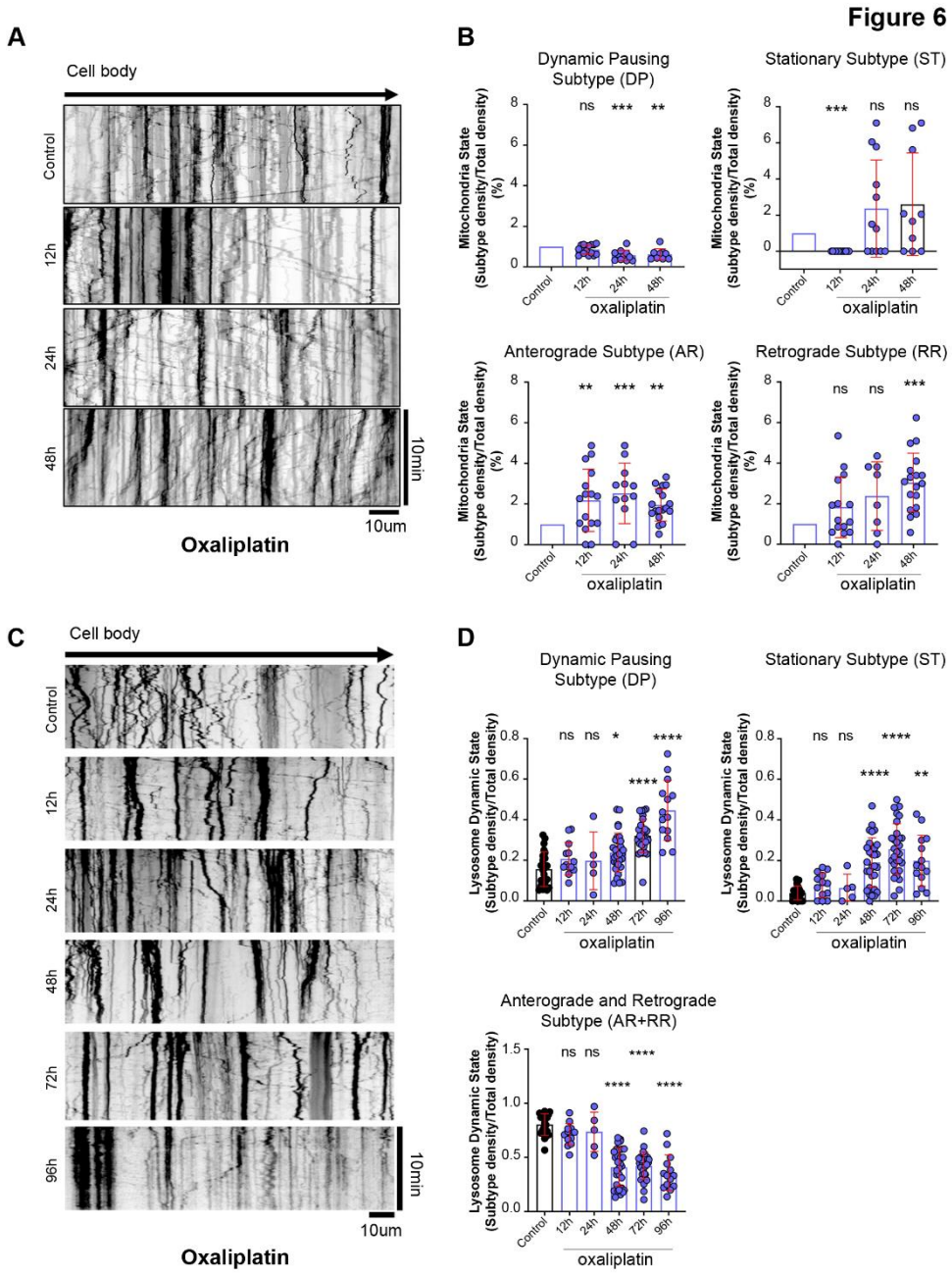
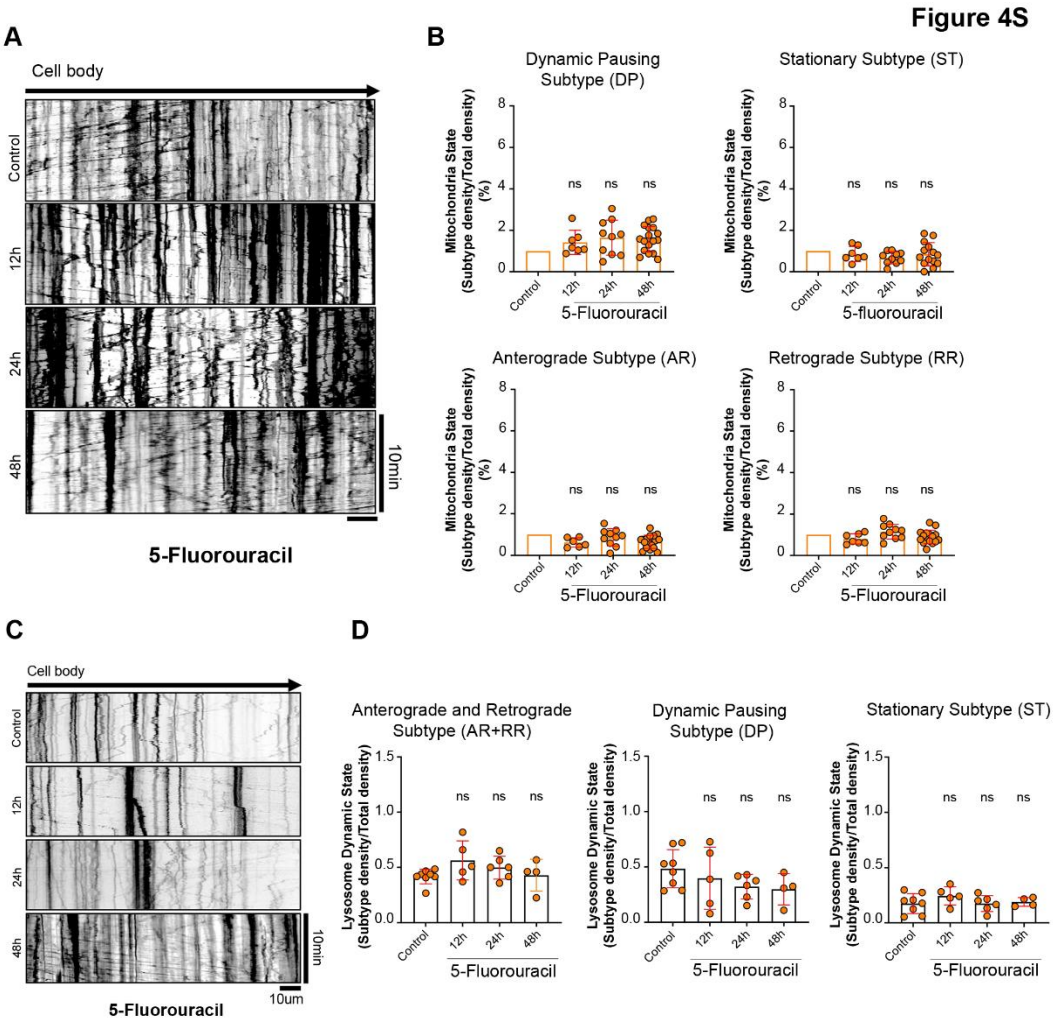


Figure 6. Oxaliplatin induces early remodeling of mitochondrial trafficking followed by progressive impairment of lysosomal trafficking in primary adult DRG neurons.

(A) Representative kymographs of mitochondrial transport in primary adult dorsal root ganglion (DRG) neurons cultured for 5 days in vitro (5 DIV), expressing Mito-DsRed and exposed to oxaliplatin (OXA; 10 nM) for 12, 24, or 48 h. Kymographs were generated from 10-min live-cell imaging recordings acquired at 2-s intervals. The arrow indicates the direction toward the cell body. Scale bars, 10 µm (horizontal) and 10 min (vertical). **(B)** Quantification of mitochondrial motility subtypes following OXA exposure. Mitochondria were classified into four motility subtypes: dynamic pausing (DP), stationary (ST), anterograde running (AR), and retrograde running (RR). The relative density of each subtype was calculated by dividing the subtype-specific mitochondrial density per unit axonal length by the total mitochondrial density per unit axonal length and expressed as a percentage of the total mitochondrial population. Each data point represents an individual axon. Data

are presented as mean ± standard deviation (SD) from four independent biological experiments. Differences among treatment conditions were assessed using the Kruskal-Wallis test followed by Dunn's multiple-comparisons test against untreated controls. Dynamic pausing was significantly reduced at 24 h (adjusted $p = 0.0007$) and 48 h (adjusted $p = 0.0079$), but not at 12 h (adjusted $p > 0.9999$). The relative density of stationary mitochondria was significantly reduced at 12 h (adjusted $p = 0.0004$), with no significant differences at 24 or 48 h (adjusted $p > 0.9999$ for both comparisons). Anterograde mitochondrial transport was significantly increased at 12 h (adjusted $p = 0.0036$), 24 h (adjusted $p = 0.0006$), and 48 h (adjusted $p = 0.0036$). Retrograde mitochondrial transport was significantly increased at 48 h (adjusted $p = 0.0001$), whereas no significant differences were detected at 12 h (adjusted $p = 0.4385$) or 24 h (adjusted $p = 0.0766$). **(C)** Representative kymographs of lysosomal transport in primary adult DRG neurons expressing LAMP1-mCherry following exposure to OXA (10 nM) for 12, 24, 48, 72, or 96 h. Kymographs were generated from 10-min live-cell imaging recordings acquired at 1-s intervals. The arrow indicates the direction toward the cell body. Scale bars, 10 μm (horizontal) and 10 min (vertical). **(D)** Quantification of lysosomal motility subtypes following OXA exposure. Lysosomes were classified as dynamically paused (DP), stationary (ST), or actively moving in the anterograde or retrograde direction (AR + RR). The relative density of each lysosomal motility subtype was calculated as the ratio of subtype-specific lysosomal density to total lysosomal density, both normalized to axonal length. Values are expressed as dimensionless ratios rather than percentages. Each data point represents an individual axon. Data are presented as mean ± SD. OXA induced a time-dependent redistribution of lysosomal motility states. The relative density of dynamically paused lysosomes increased significantly at 48 h (adjusted $p = 0.0165$), 72 h (adjusted $p < 0.0001$), and 96 h (adjusted $p < 0.0001$), whereas no significant differences were detected at 12 or 24 h. Similarly, stationary lysosomes increased significantly at 48 h (adjusted $p < 0.0001$), 72 h (adjusted $p < 0.0001$), and 96 h (adjusted $p = 0.0019$). In contrast, the relative density of actively moving lysosomes (AR + RR) was significantly reduced at 48, 72, and 96 h (adjusted $p < 0.0001$ for all comparisons), with no significant differences at earlier time points. Statistical comparisons were performed using ordinary one-way ANOVA followed by Dunnett's multiple-comparisons test for DP ($F(5, 108) = 18.58$, $p < 0.0001$), and Welch's ANOVA followed by Dunnett's T3 multiple-comparisons test for ST ($W(5, 26.90) = 22.82$, $p < 0.0001$) and AR + RR ($W(5, 27.33) = 43.55$, $p < 0.0001$). For panels B and D, all reported pairwise p-values were adjusted for multiple comparisons. Statistical significance: *$p < 0.05$, **$p < 0.01$, ***$p < 0.001$, ****$p < 0.0001$; ns, not significant.



Supplementary Figure S4. Effects of 5-fluorouracil on mitochondrial and lysosomal trafficking in primary adult DRG neurons.

(A) Representative kymographs of mitochondrial transport in primary adult dorsal root ganglion (DRG) neurons expressing Mito-DsRed and exposed to 5-fluorouracil (5-FU) for 12, 24, or 48 h, together with untreated controls. Kymographs were generated from 10-min live-cell imaging recordings acquired at 2-s intervals. The arrow indicates the direction toward the cell body. Scale bars, 10 µm (distance) and 10 min (time). **(B)** Quantification of mitochondrial motility subtypes following 5-FU exposure. Mitochondria were classified into four motility states: dynamic pausing (DP), stationary (ST), anterograde running (AR), and retrograde running (RR). The relative density of each subtype was calculated as the ratio of subtype-specific mitochondrial density to total mitochondrial density, both normalized to axonal length, and expressed as a percentage of the total mitochondrial population. Each data point represents an individual axon. Data are presented as mean ± standard deviation (SD) from four independent biological experiments. Differences among treatment conditions were assessed using the Kruskal–Wallis test followed by Dunn's multiple-comparisons test against untreated controls. For dynamic pausing (DP), no significant overall difference was detected ($H(3) = 5.920$, $p = 0.1156$). Comparisons with untreated controls were not significant at 12 h (adjusted $p = 0.5087$), 24 h (adjusted $p = 0.2498$), or 48 h (adjusted $p = 0.1607$). For stationary mitochondria (ST), no significant overall difference was detected ($H(3) = 2.417$, $p = 0.4905$). Dunn's multiple-comparisons test revealed no significant differences at 12 h (adjusted $p > 0.9999$), 24 h (adjusted $p = 0.3681$), or 48 h (adjusted $p = 0.7575$). For anterograde mitochondrial transport (AR), the overall Kruskal–Wallis test indicated a significant difference among groups ($H(3) = 7.969$, $p = 0.0467$). However, Dunn's multiple-comparisons test did not identify significant

differences relative to untreated controls at 12 h (adjusted p = 0.0896), 24 h (adjusted p = 0.9748), or 48 h (adjusted p = 0.0653). For retrograde mitochondrial transport (RR), no significant overall difference was detected ($H(3) = 4.937$, $p = 0.1764$). No significant differences were observed at 12 h (adjusted p = 0.7323), 24 h (adjusted p > 0.9999), or 48 h (adjusted p > 0.9999). **(C)** Representative kymographs of lysosomal transport in primary adult DRG neurons expressing LAMP1-mCherry following exposure to 5-FU for 12, 24, or 48 h, together with untreated controls. Kymographs were generated from 10-min live-cell imaging recordings acquired at 1-s intervals. The arrow indicates the direction toward the cell body. Scale bars, 10 μm (distance) and 10 min (time). **(D)** Quantification of lysosomal motility states following 5-FU exposure. Lysosomes were classified as actively moving in the anterograde or retrograde direction (AR + RR), dynamically paused (DP), or stationary (ST). The relative density of each lysosomal motility subtype was calculated as the ratio of subtype-specific lysosomal density to total lysosomal density, both normalized to axonal length. Values are expressed as dimensionless ratios rather than percentages. Each data point represents an individual axon. Data are presented as mean ± SD. Differences among treatment conditions were assessed using the Kruskal–Wallis test followed by Dunn's multiple-comparisons test against untreated controls. No statistically significant differences in lysosomal motility states were detected following 5-FU exposure at 12, 24, or 48 h. For panels B and D, statistical significance was defined as $p < 0.05$. Adjusted p-values are reported for post hoc comparisons; ns, not significant.

DISCUSSION

Chemotherapy-induced peripheral neuropathy (CIPN) remains one of the most frequent dose-limiting toxicities of anticancer treatment and represents a major clinical challenge because it often necessitates dose reduction or treatment discontinuation, compromising therapeutic efficacy and quality of life. Although several mechanisms have been implicated in CIPN, including oxidative stress, mitochondrial dysfunction, altered axonal transport, and cytoskeletal remodeling, the sequence of events that drives peripheral nerve degeneration remains incompletely understood. An additional unresolved question is why certain chemotherapeutic agents, such as platinum compounds, consistently induce peripheral neuropathy, whereas others with distinct mechanisms of action produce little or no neurotoxicity despite exposing sensory neurons to substantial metabolic stress.

To address this question, we directly compared oxaliplatin (Oxa), a platinum-based chemotherapeutic strongly associated with chronic sensory neuropathy, with 5-fluorouracil (5-FU), an antimetabolite commonly co-administered in colorectal cancer treatment but rarely associated with clinically significant peripheral neurotoxicity. By integrating complementary in vivo and in vitro approaches, we investigated the temporal relationship among oxidative stress, mitochondrial bioenergetics, tubulin post-translational modifications (PTMs), intracellular organelle trafficking, and axonal degeneration. Our findings demonstrate that although both Oxa and 5-FU induce early mitochondrial bioenergetic dysfunction in primary sensory neurons, only Oxa elicits oxidative stress in sensory ganglia in vivo, selective polyglutamylated tubulin accumulation in vitro and in vivo, and progressive remodeling of mitochondrial and lysosomal trafficking that precedes sensory axon degeneration in primary neurons. These observations identify selective in vivo oxidative stress, downregulation of terminal oxidative phosphorylation, mitochondrial trafficking and tubulin-code remodeling, rather than loss of mitochondrial potential and respiration alone, as distinguishing features of Oxa-induced neurotoxicity and provide a new framework for understanding the cellular mechanisms underlying platinum-induced peripheral neuropathy.

Chronic Oxa treatment increased lipid peroxidation selectively within dorsal root ganglia (DRG), as evidenced by elevated TBARS levels, while simultaneously reducing the expression of major antioxidant defense enzymes, including SOD1, SOD2, catalase, and glutathione reductase. The restriction of oxidative damage to sensory ganglia, together with the absence of changes in plasma or

sciatic nerve, suggests that DRG neuronal cell bodies represent a primary site of Oxa-induced oxidative stress rather than reflecting a generalized systemic response to chemotherapy. These observations are consistent with previous studies identifying DRG neurons as particularly vulnerable to platinum accumulation because of their fenestrated vasculature, high metabolic demand, and limited antioxidant capacity (Cavaletti et al., 2011; Areti et al., 2014).

We found that oxidative stress induced by Oxa was accompanied by selective remodeling of mitochondrial oxidative phosphorylation. Rather than producing a generalized loss of mitochondrial proteins, Oxa selectively reduced the expression of the Complex IV subunit mt-COX2 and the ATP synthase subunit ATP5A1, whereas proteins associated with Complexes I, II, and III remained largely unchanged. This pattern argues against widespread mitochondrial depletion and instead suggests preferential impairment of the terminal components of the respiratory chain responsible for maintaining mitochondrial membrane potential and ATP production (Nunnari and Suomalainen, 2012; Wallace et al., 2013; Spinelli and Haigis, 2018). We can speculate that the selective reduction of mt-COX2 reflects the particular susceptibility of mitochondrial DNA-encoded respiratory subunits to platinum-induced mitochondrial DNA damage and oxidative stress, whereas preservation of Complexes I–III indicates that OXPHOS remodeling occurs in a highly selective rather than indiscriminate manner (Suomalainen and Battersby, 2018; Marullo et al., 2013). Importantly, these alterations were already evident before the development of the most severe behavioral and structural manifestations of neuropathy, supporting the concept that localized OXPHOS remodeling is an early component of the neuronal response to Oxa. The functional relevance of these observations was further explored in primary adult DRG neurons, where Oxa induced progressive mitochondrial depolarization together with reduced basal respiration, maximal respiratory capacity, and ATP-linked respiration prior to axonal degeneration. Unexpectedly, however, the same bioenergetic parameters were also impaired following 5-FU exposure, despite the absence of behavioral deficits, axonal degeneration, or alterations in organelle trafficking. This comparison represents one of the central findings of the present study because it indicates that mitochondrial bioenergetic dysfunction, although an early consequence of chemotherapeutic exposure, is not sufficient by itself to determine whether sensory neurons progress toward degeneration. Instead, our data suggest that additional Oxa-specific mechanisms must couple mitochondrial stress to the downstream cellular events that ultimately culminate in peripheral neuropathy.

Another major finding of the present study is the identification of selective tubulin-code remodeling as a distinguishing feature of Oxa-induced neurotoxicity. Although both Oxa and 5-FU induced comparable mitochondrial bioenergetic impairment, only Oxa promoted the accumulation of polyglutamylated tubulin in vivo and in cultured sensory neurons. In contrast, the other major tubulin PTMs examined, including acetylated, detyrosinated, and Δ2 tubulin, remained unchanged following Oxa treatment, indicating that platinum exposure does not induce a generalized remodeling of the tubulin PTM landscape but instead selectively targets polyglutamylation. This selective response was further underscored by the absence of any detectable changes in tubulin PTMs following 5-FU treatment despite comparable impairment of mitochondrial membrane potential and oxidative phosphorylation. Together, these findings identify polyglutamylation as one of the earliest molecular events that differentiates the neurotoxic response to Oxa from the more limited cellular stress induced by 5-FU. Indeed, tubulin polyglutamylation has emerged as a key regulator of microtubule function and is increasingly recognized as a molecular "traffic-control" mechanism that modulates motor protein processivity, cargo selection, microtubule-associated protein interactions, and the activity of microtubule-severing enzymes (Janke and Magiera, 2020; Bodakuntla et al., 2021). Unlike structural modifications that primarily affect microtubule stability, polyglutamylation fine-tunes the interaction of kinesin, dynein, and microtubule-associated proteins with the microtubule lattice, thereby regulating intracellular cargo transport in a highly selective manner. Consistent with this concept, dysregulated polyglutamylation has been implicated in several neurodegenerative disorders and in animal models carrying mutations in cytosolic carboxypeptidases (CCPs), the enzymes responsible for tubulin deglutamylation, where excessive glutamylation disrupts axonal transport and promotes

neuronal degeneration (Rogowski et al., 2010; Shashi et al., 2018). Interestingly, recent evidence indicates that remodeling of the tubulin code by CIPN-promoting drugs is not restricted to neurons. Horibata and colleagues recently demonstrated that cisplatin-resistant ovarian cancer cells undergo extensive remodeling of tubulin isotypes and PTMs, including increased tubulin glutamylation, together with altered microtubule dynamics and stabilization (Horibata et al., 2026). Although these studies were performed in cancer cells and addressed mechanisms of chemoresistance rather than neurotoxicity, they support the concept that platinum compounds can induce selective remodeling of the tubulin code across distinct cellular contexts. Our findings extend this concept to primary sensory neurons, where polyglutamylation emerges during the development of Oxa-induced neurotoxicity, coincides with altered organelle trafficking, and precedes overt axonal degeneration. Together, these observations suggest that remodeling of the tubulin code may represent a conserved cellular response to platinum-based agents, although its downstream functional consequences are highly cell type-dependent, promoting chemoresistance in tumor cells while contributing to neuronal dysfunction in sensory neurons.

Our findings do not establish a direct causal relationship between localized OXPHOS impairment and mitochondrial transport or tubulin-code remodeling. Indeed, the comparison with 5-FU indicates that mitochondrial bioenergetic stress alone is insufficient to trigger remodeling of the tubulin code or axonal degeneration. Instead, Oxa appears to engage additional signaling pathways that selectively promote early mitochondrial transport remodeling followed by tubulin hyperpolyglutamylation, thereby identifying this modification as a candidate molecular switch linking platinum-induced cellular stress to downstream disruption of neuronal homeostasis. Live-cell imaging further revealed an Oxa-induced, staged reorganization of intracellular organelle trafficking. Rather than producing an immediate collapse of axonal transport, Oxa initially promoted a dynamic redistribution of mitochondrial motility characterized by reduced pausing and enhanced anterograde transport, followed by a delayed increase in retrograde mitochondrial movement. This temporal sequence suggests that mitochondrial trafficking is actively remodeled during the early phases of neuronal stress rather than being passively disrupted as a consequence of cellular injury. In contrast, lysosomal trafficking remained largely preserved during the initial stages of Oxa exposure but became progressively impaired after prolonged treatment, indicating that different organelles exhibit distinct temporal responses to platinum-induced stress. Within this framework, late lysosomal transport defects may arise as a downstream consequence of sustained tubulin hyperpolyglutamylation, further reinforcing the idea that selective tubulin-code remodeling contributes to the transition from early compensatory responses to maladaptive organelle trafficking and axonal degeneration.

The early increase in mitochondrial motility observed following Oxa treatment is consistent with current concepts of neuronal mitochondrial quality control. Mitochondria continuously undergo dynamic redistribution to match local metabolic demand and to facilitate the repair, redistribution, or removal of damaged organelles (Misgeld and Schwarz, 2017; Sheng and Cai, 2012). Increased anterograde transport during the early stages of Oxa exposure may therefore represent an adaptive attempt to maintain ATP supply within distal axons, whereas the subsequent increase in retrograde transport is compatible with the retrieval of dysfunctional mitochondria toward the cell body for quality-control processes, including mitophagy. Although our data do not directly address the molecular pathways regulating these trafficking changes, their temporal relationship with selective polyglutamylation raises the possibility that remodeling of the tubulin code contributes to fine-tuning motor protein activity during the neuronal response to platinum-induced stress.The delayed impairment of lysosomal trafficking further supports the concept that mitochondrial and lysosomal responses are mechanistically distinct. Lysosomes play central roles in autophagy, organelle turnover, and degradation of damaged cellular components, and disruption of their transport has been implicated in numerous neurodegenerative disorders (Ferguson et al., 2019; Pu et al., 2016). The preservation of lysosomal motility during the early phases of Oxa exposure, followed by its progressive impairment, suggests that lysosomal dysfunction is unlikely to initiate neuronal injury but may instead contribute to the progressive failure of intracellular quality-control mechanisms as

cellular stress persists. Together, these findings support a model in which mitochondrial trafficking undergoes an early adaptive remodeling, whereas lysosomal transport becomes compromised only during later stages of neuronal dysfunction. One of the most intriguing observations emerging from the present study is that these trafficking alterations were not reproduced by 5-FU. Despite inducing mitochondrial depolarization and impaired oxidative phosphorylation comparable to those observed following Oxa treatment, 5-FU failed to alter either mitochondrial or lysosomal trafficking. This comparison substantially strengthens the mechanistic interpretation of our findings by demonstrating that impaired mitochondrial bioenergetics alone is insufficient to trigger the profound reorganization of intracellular transport observed following Oxa exposure. Instead, our data support the existence of an Oxa-specific adaptive program in which organelle trafficking is selectively remodeled before the onset of overt neuronal degeneration.

By distinguishing mechanisms associated with general chemotherapeutic stress from those specifically associated with neurotoxicity, our study provides a new conceptual framework for understanding the pathogenesis of platinum-induced peripheral neuropathy. More broadly, these findings identify localized OXPHOS, mitochondrial transport and tubulin code remodeling as a promising therapeutic targets to maintain axonal integrity, and ultimately prevent CIPN induced by Oxa.

MATERIAL AND METHODS

Animal model.

Male Wistar rats (Envigo, Udine, Italy) were used. Animal care and husbandry were conducted in accordance with institutional guidelines and in compliance with national (D.L.vo No. 26/2014) and international laws and policies (EEC Council Directive 86/609, OJ L 358, 1, Dec. 12, 1987; Guide for the Care and Use of Laboratory Animals, U.S. National Research Council, 1996). The study protocol was approved by the Ethics Committee of the University of Milano-Bicocca (authorization No. 0041156/21) and by the Italian Ministry of Health (authorization No. 449/2020-PRA total of 189 animals were randomized across three experimental time points: 24 h after the first injection (acute treatment), mid-treatment (2 weeks for 5-fluorouracil [5-FU] and 3 weeks for oxaliplatin [Oxa]), and end of treatment (4 weeks for 5-FU and 6 weeks for Oxa). At each time point, animals were assigned to three treatment groups (n=21/group): Control receiving 5% glucose solution intravenously (i.v.); Oxa, receiving oxaliplatin at 5 mg/kg i.v. twice weekly; and 5-FU, receiving 5-fluorouracil at 50 mg/kg i.v. once weekly Animals were housed two to three per cage in a certified, limited-access facility under controlled temperature (21 ± 2 °C) and humidity (50 ± 20%), with a 12-h light/dark cycle (lights on from 7:00 a.m. to 7:00 p.m.). Animals were monitored daily for mortality, and general health and body weight were assessed twice weekly throughout the treatment period. Body weight was also used to adjust drug doses as required. At each experimental time point, all animals (n= 21/group) underwent behavioral and neurophysiological assessments, while tissues from n= 7 animals/group were collected for subsequent analyses.

Dynamic test

Mechanical sensitivity was assessed using a Dynamic Aesthesiometer (model 37450, Ugo Basile Biological Instruments, Comerio, Italy). The test was performed at baseline, before treatment allocation (data not shown), and 24 h after the first injection in the acute experimental setting. In the chronic experimental setting, assessments were performed at the end of treatment (4 weeks for 5-FU and 6 weeks for Oxa), as previously described (Tarasiuk et al., 2026). Following a brief acclimatization period, a metallic filament was positioned beneath the plantar surface of each hind paw. The filament applied progressively increasing pressure, reaching a maximum of 50 g over 20 s, until a paw withdrawal response was elicited. Three measurements were obtained from each hind paw, and the mean of the six measurements was calculated for each animal. Mechanical withdrawal thresholds were expressed in grams (g).

Cold plate
Cold sensitivity was assessed using a Cold Plate apparatus (model 35100, Hot/Cold Plate, Ugo Basile Biological Instruments, Comerio, Italy), consisting of a Plexiglas cylinder positioned on a thermostatically controlled plate maintained at 4 °C.
The test was performed at baseline, before treatment allocation (data not shown), and 24 h after the first injection in the acute experimental setting. In the chronic experimental setting, assessments were performed at the end of treatment (4 weeks for 5-FU and 6 weeks for Oxa), as previously described (Marmiroli et al., 2017).
Briefly, each animal was placed individually in the Plexiglas enclosure and allowed to move freely. An observer recorded the number of cold-evoked nocifensive responses, including hind paw lifting, flicking, licking, and jumping, during a 5-min observation period. The test was immediately terminated if the animal exhibited signs of severe distress, including pronounced anxiety or vocalization.

Neurophysiological examination
Nerve conduction velocity (NCV) and sensory nerve action potential (SNAP) amplitude were assessed in the caudal and digital nerves to evaluate the development of peripheral neuropathy following chronic administration of Oxa and 5-FU.Neurophysiological recordings were performed using an electromyography system (Matrix Light, Micromed, Treviso, Italy). Assessments were conducted only in the chronic experimental setting, at baseline, before treatment allocation (data not shown), and at the end of treatment. A pair of needle recording electrodes was positioned at the base of the tail for caudal nerve recordings or near the ankle for digital nerve recordings. Stimulating electrodes were placed approximately 3 cm from the recording site for caudal nerve measurements or near the fourth toe for digital nerve measurements. Latencies were measured from stimulus onset, and peak-to-peak amplitudes were determined. NCV was calculated by dividing the distance between the stimulating and recording electrodes by the onset latency measured from the stimulus artifact. Stimulation intensity, duration, and frequency were adjusted to obtain reproducible responses with maximal amplitudes.
All neurophysiological examinations were performed under isoflurane anesthesia, with continuous monitoring of vital signs.

Intraepidermal nerve fiber (IENF) density analysis

In both experimental settings, skin biopsies were collected from the plantar surface of the hind paws to assess intraepidermal nerve fiber (IENF) density. Samples were immediately fixed in 2% periodate-lysine-paraformaldehyde (PLP) fixative for 24 h, cryoprotected, and stored at −20 °C until processing. Skin samples were serially sectioned at a thickness of 20 µm and immunostained using a free-floating protocol with a rabbit polyclonal antibody against protein gene product 9.5 (PGP9.5; Proteintech, Rosemont, IL, USA), as previously described (Pozzi et al., 2023) Images were acquired using a 20-megapixel USB 3.0 digital camera (TiesseLab; TiEsseLab Srl, Milan, Italy) mounted on a light microscope (Nexcope NE920 AUTO; TiEsseLab Srl, Milan, Italy). The total number of PGP9.5-positive nerve fibers crossing the dermal–epidermal junction was manually counted in real time at 40× magnification. IENF density was calculated as the number of nerve fibers crossing the dermal–epidermal junction per millimeter of epidermal length (fibers/mm).

Isolation of Adult DRG Neurons. All animal procedures were conducted in accordance with the National Institutes of Health (NIH) Guide for the Care and Use of Laboratory Animals and were approved by the Institutional Animal Care and Use Committee (IACUC) of Columbia University (protocol No. AC-AABZ7700). Dorsal root ganglia (DRG) were isolated from 8-10-week-old male

C57BL/6J mice, dissociated, and plated in live-imaging dishes or XF24-well microplates, as previously described (Pero ME., 2021; Shin G., 2021). Briefly, the spinal column was isolated immediately after euthanasia and divided into approximately two pieces, which were then cut along the midline to expose the DRG for isolation. Each piece was dissected within 7 min, while the remaining tissue was kept on ice. DRG from the cervical, thoracic, and lumbar regions were collected and immediately placed in HBSS (Life Technologies) or DMEM (Life Technologies) on ice.
After collection, visible axonal tracts were carefully removed, and the DRG were incubated in 1 mg/mL collagenase A (Sigma) for 1 h at 37 °C. Following incubation, the DRG were washed twice with DMEM and subsequently digested with 0.05% trypsin (Life Technologies) in DMEM for 2 min at 37 °C. After enzymatic digestion, the cells were washed twice with Neurobasal medium supplemented with 2% B-27 (Invitrogen), 0.5 mM glutamine (Invitrogen), 10% fetal bovine serum (FBS; Sigma), and 100 U/mL penicillin-streptomycin. DRG neurons were then dissociated by repeated gentle pipetting until no visible cell clumps remained. Following dissociation, cells were resuspended in supplemented Neurobasal medium containing 10% FBS to a final volume of 1.2 mL (100 µL × 12 wells) and plated onto dishes that had been coated overnight with 100 µg/mL poly-D-lysine (Sigma) at 37 °C, followed by 10 µg/mL laminin (Life Technologies) for 1 h at 37 °C.
After 30 min, 500–1000 µL of supplemented Neurobasal medium was gently added to each well without disturbing the plated cells. At 4-5 days in vitro (DIV), 1 µL of a 1000× stock solution of oxaliplatin (Oxa) or 5-fluorouracil (5-FU) was added to each well containing 1 mL of medium, resulting in final concentrations of 10 nM Oxa and 500 nM 5-FU, respectively. An equivalent volume (1 µL) of DMSO was added to control wells as a vehicle control.

Thiobarbituric Acid-Reactive Substance. Plasma, DRG and sciatic nerve thiobarbituric acid-reactive substances (TBARS) assay was performed as an indirect index of reactive oxygen species (ROS) production. TBARS levels analyses were measured on whole DRG and sciatic nerves homogenates, the specific cellular source of oxidative stress (neuronal versus non-neuronal cells) cannot be determined from these experiments. This method measures lipid peroxidation, which is positively correlated with the ROS amount. The assay was performed as published previously (Giatti S., et al., 2015) Briefly, 400 µL of lysis buffer (Tris-HCl 0.1 M, pH 7.4; EDTA 1.34 mM; glutathione 0.65 mM) was added to 10 µg of tissue for homogenization. Then, 100 µL of homogenate or 100 µL in case of plasma was incubated at 95 °C for 1 h with a solution containing 600 µL of phosphoric acid 1% and 200 µL of TBA 0.6%. After incubation, samples were cooled to RT and 1 mL of n-butanol was added. Then, the extraction of TBARS was obtained with centrifugation at 1200x g at 4°C for 20 min to obtain the supernatant that was then collected and analyzed fluorometrically at an excitation wavelength of 532 nm and an emission wavelength of 553 nm. Quantification was performed using the standard curve prepared with malondialdehyde following similar conditions. Then, the obtained amount was normalized based on protein content for each sample, detected by Bradford assay. For plasma, the TBARS assay value was normalized for the volume of sample used for analysis.

Real Time PCR. Gene expression was evaluated on total RNA extracted from frozen tissues using Trizol Trizol (Invitrogen, San Giuliano Milanese, Italy) and Direct-zol TM RNA MiniPrep kit (Zymo Research, Irvine, Calif., USA). Quantified RNA was analyzed using a TaqMan quantitative real-time PCR instrument (CFX96 real time system; Bio-Rad Laboratories, Segrate, Italy) in duplicate and as multiplexed reactions in a 96-well format. 36B4 was used as housekeeping gene. Specific TaqMan MGB probes and primers sequence were purchased at Eurofins MWG-Operon (Milano, Italy) and are available on request: 36B4 (forward: GGATGACTACCCAAAATGCTTC; reverse: TGGTGTTCTTGCCCATCAG); CAT (forward: CTCAGGTGCGGACATTCTATAC; reverse: GACCGCTTTCCTCTGAATGA); GSR (forward: GTCTGTGGGAAAGCACTTCT; reverse: CACGGTAGGGATGTTGTCATAG). Specific TaqMan MGB probes (Applied Biosystems, Thermo Fisher Schientific) were: Sod1 (Rn00566938-m1) and Sod2 (Rn00690588-g1).

Seahorse bioenergetic analysis

Mitochondrial respiration in primary dorsal root ganglion (DRG) neurons was assessed using a Seahorse Bioscience XF24 extracellular flux analyzer, as previously described (Morcillo et al., 2024). Cells were seeded at a density of 4×10^4 cells/well in XF24 microplates. Before measurements, cells were washed and incubated in XF base medium (Agilent Technologies, Cat. No. 102353-100) supplemented with 25 mM glucose and 2 mM sodium pyruvate (Thermo Fisher Scientific, Cat. No. 11360070), adjusted to pH 7.4. Following incubation for 45 min at 37 °C in a CO_2-free incubator, oxygen consumption rate (OCR) was measured under basal conditions and after sequential injections of oligomycin (1 μM; ATP synthase inhibitor; Sigma-Aldrich, Cat. No. 75351), carbonyl cyanide-p-trifluoromethoxyphenylhydrazone (FCCP; 0.75 μM; mitochondrial uncoupler; Sigma-Aldrich, Cat. No. C2920), and rotenone and antimycin A (1 μM each; mitochondrial complex I and III inhibitors, respectively; Sigma-Aldrich, Cat. Nos. R8875 and A8674).Basal respiration, maximal respiration, and ATP-linked respiration were determined from the OCR measurements. ATP-linked respiration was calculated as the difference between basal OCR and OCR following oligomycin injection. OCR values were normalized to total protein content measured at the end of each experiment. Measurements were performed using at least three technical replicates per condition across 3-4 independent biological experiments. Data were analyzed using the Wave Report Generator software (Agilent Technologies).

Mitochondrial membrane potential analysis

Mitochondrial membrane potential was assessed using tetramethylrhodamine methyl ester (TMRM; T668, Invitrogen), a cell-permeant fluorescent probe that accumulates in polarized mitochondria in a membrane potential-dependent manner. Primary dorsal root ganglion (DRG) neurons were treated with oxaliplatin (10 nM) or 5-fluorouracil (5-FU, 500 nM) for 12, 24, and 48 h. Untreated neurons served as controls. Cultured neurons were incubated with TMRM at a final concentration of 50 nM in prewarmed medium for 30 min at 37 °C, protected from light. Following incubation, cells were gently washed twice with prewarmed Live Imaging Medium (Hank's Balanced Salt Solution [HBSS]; Corning, Cat. No. 21-023-CV, supplemented with 10 mM HEPES and 60 mM glucose) to remove excess dye and maintained in the same medium throughout image acquisition.

Live-cell fluorescence imaging was performed using an Olympus IX81 epifluorescence microscope equipped with a monochrome CCD camera (Sensicam QE; Cooke Corporation) and a 60× objective. TMRM fluorescence was detected using an RFP/TRITC filter set (excitation approximately 548 nm; emission approximately 574 nm). Identical acquisition settings were maintained across experimental groups. Images were analyzed using ImageJ software.. Individual mitochondria along neuronal axons were manually selected as regions of interest (ROIs), and mean TMRM fluorescence intensity was measured at the same time point for all experimental conditions to minimize photobleaching-related variability. Fluorescence values from individual mitochondria were averaged for each neurite. Approximately 160 mitochondria across 10-16 neurites per experimental condition were analyzed from four independent experiments.

Overall, 57 neurites were included in the oxaliplatin analysis and 62 in the 5-FU analysis. The mitochondrial uncoupler carbonyl cyanide-p-trifluoromethoxyphenylhydrazone (FCCP) was used as a positive control for mitochondrial membrane depolarization.

Quantitative Immunoblotting and Immunofluorescence Analysis of Tubulin PTMs and OXPHOS Proteins

Western Blotting. Whole-cell lysates from cultured dorsal root ganglion (DRG) neurons and DRG and sciatic nerve tissues dissected from treated animals were prepared by manual homogenization in

2× Laemmli buffer, followed by sonication (Branson Sonifier 250, 15 s), heating at 95 °C for 5 min, and a brief centrifugation (1-2 min) to remove insoluble debris prior to gel loading.
Proteins were separated on 10% Bis-Tris gels (Invitrogen) and transferred onto nitrocellulose membranes. Following blocking with 5% nonfat milk in TBS, membranes were incubated with primary antibodies overnight at 4 °C or for 1 h at 37 °C, followed by incubation with the appropriate secondary antibodies for 1 h at room temperature. For infrared fluorescence detection, membranes were incubated with DyLight 680 or DyLight 800 conjugated secondary antibodies (Rockland Immunochemicals), and signals were acquired using an Odyssey infrared imaging system (LI-COR Biosciences). Band intensities were quantified using Fiji (ImageJ; National Institutes of Health, USA). For OXPHOS protein detection, horseradish peroxidase (HRP)-conjugated secondary antibodies and enhanced chemiluminescence (ECL) were used. Chemiluminescent signals were acquired using a ChemiDoc XRS+ system (Bio-Rad, Segrate, Italy) and analyzed using Image Lab software (version 5.2.1; Bio-Rad).Within each independent experiment, the mean control value was set to 100%, and protein expression levels were expressed as percentages of the corresponding control.

Immunofluorescence Staining
For immunofluorescence analysis of tissue specimens, paraffin-embedded DRG (L4–L5) and sciatic nerve samples were sectioned at 7 µm thickness. Sections were deparaffinized in xylene (2 × 7 min), rehydrated through a graded ethanol series (100%, 90%, 80%, 60%, and 40%; 5 min each), and immersed in distilled water for 5 min. Following two washes in PBS (10 min each), antigen retrieval was performed by heating sections in 10 mM citrate buffer (pH 6.0) for 15 min. Sections were allowed to cool for 15 min, washed three times with PBS, permeabilized with 0.01% Triton X-100 for 10 min, and blocked with 10% normal goat serum (NGS; Thermo Fisher Scientific) in PBS for 1 h at room temperature. Primary antibodies were diluted in 10% NGS/PBS and incubated overnight at 4 °C.
For immunofluorescence analysis of cultured DRG neurons, cells were fixed with 4% paraformaldehyde for 15 min, permeabilized with 0.1% Triton X-100 for 10 min, blocked with 10% NGS for 30 min, and incubated overnight with primary antibodies as previously described.
For both tissue sections and cultured neurons, Alexa Fluor-conjugated secondary antibodies were diluted 1:200 in 10% NGS/PBS and incubated for 1 h at room temperature.

Immunofluorescence Image Acquisition and Quantification
Images of immunostained primary DRG neuronal cultures and DRG and sciatic nerve sections from treated animals were acquired using an Olympus IX81 epifluorescence microscope equipped with a 20× objective lens. Image analysis was performed using Fiji (ImageJ; National Institutes of Health, USA). For quantification of tubulin post-translational modifications (PTMs) in DRG sections, individual neuronal cell bodies were manually outlined using the freehand selection tool in ImageJ to define regions of interest (ROIs). For each ROI, fluorescence intensities corresponding to the PTM-specific signal and βIII-tubulin were measured within the same selected area. PTM levels were expressed as the ratio of PTM to βIII-tubulin fluorescence intensity.
The same quantification approach was applied to sciatic nerve sections, where ROIs were defined around axonal bundles.

Primary and Secondary Antibodies. The following primary antibodies were used for Western blotting (WB) and immunofluorescence (IF): Detyrosinated α-tubulin: rabbit polyclonal (1:200 IF; 1:2,000 WB; Millipore, Cat. No. AB3201, RRID: AB-177350). Tyrosinated α-tubulin: rat monoclonal, clone YL1/2 (1:400 IF; 1:2,000 WB; Millipore, Cat. No. MAB1864, RRID: AB-2210391). Acetylated α-tubulin: mouse monoclonal, clone 6-11B-1 (1:300 IF; 1:2,000 WB; Sigma-Aldrich, Cat. No. T7451, RRID: AB-609894). Δ2-tubulin: rabbit polyclonal (1:400 IF; 1:1,000 WB; Millipore, Cat. No. AB3203, RRID: AB-177351). Polyglutamylated tubulin (polyE): rabbit polyclonal, IN105 (1:2,000 WB; AdipoGen, Cat. No. AG-25B-0030, RRID: AB-2490540). βIII-

tubulin: mouse monoclonal (Abcam, Cat. No. Ab78078) and rabbit polyclonal (Abcam, Cat. No. Ab18207), used at 1:500 for IF and 1:2,000 for WB. GAPDH: mouse monoclonal (1:5,000 WB; Thermo Fisher Scientific, Cat. No. MA5-36097) and rabbit polyclonal (1:10,000 WB; Santa Cruz Biotechnology, Cat. No. Sc-25778, RRID: AB-10167668). Neurofilament 200 (NF200): chicken polyclonal (1:200 IF; Aves Labs, Cat. No. NFH). OXPHOS proteins: mouse anti-OXPHOS antibody (Abcam, Cat. No. Ab10413). For infrared Western blot detection, the following secondary antibodies were used: Fluorescent TrueBlot anti-rabbit IgG DyLight 800 (mouse monoclonal, clone eB182, 1:10,000; Rockland Immunochemicals, Cat. No. 18-4516-32, RRID: AB-2610841) and goat anti-mouse IgG (H&L), DyLight 680-conjugated (Rockland Immunochemicals, Cat. No. 610-144-002, RRID: AB-11183140). For chemiluminescent Western blot detection, HRP-conjugated secondary antibodies were used. For immunofluorescence, Alexa Fluor-conjugated secondary antibodies were used as described above.

Antibody Specificity and Validation
Antibodies recognizing tubulin post-translational modifications (PTMs) were selected based on their reported specificity for the corresponding modified epitopes, manufacturers' characterization data, and previous experience in our laboratory (Qu et al, 2017; Pero et al., 2021; Martínez-Hernándezet al., 2022; Peris et al., 2022; Iseppon et al., 2026). Antibody performance had been previously evaluated by Western blot analysis using different biological samples, including immortalized cell lines, brain tissues, and primary neuronal cultures. These analyses consistently revealed immunoreactive bands at approximately 50 kDa, corresponding to the expected molecular weight of tubulin, supporting the reliability and reproducibility of antibody recognition across different experimental models. Furthermore, as shown in the full-length, uncropped Western blot images provided in the Supplementary Materials, no additional nonspecific bands were detected in the vicinity of the expected tubulin bands, further supporting the selectivity of antibody recognition under the experimental conditions used. No additional antibody-specific validation experiments were performed as part of the present study.

Degeneration Index Measurements in DRG Neurons. Images of an average of 10 random fields of dissociated adult DRG neurons fixed and immunostained with mouse anti-neurofilament antibody were acquired using a 20× objective lens (Olympus IX81) coupled to a monochrome charge-coupled device camera (Sensicam QE; Cooke Corporation). To quantify axonal degeneration, the areas occupied by the axons (total axonal area) and degenerating axons (fragmented axonal area) were measured in the same field. Images were automatically thresholder (global threshold) using a default auto threshold method, binarized, and the fragmented axonal area measured by using the particle analyzer module of ImageJ (size of small fragments = 20 to 10,000 pixels). Degeneration index was calculated as the ratio between the fragmented axonal area and the total axonal area (Pero ME., et al., 2021; Shin GJ et al., 2021; Bosc L, et al., 2025; Gerdts J., et al., 2011).

Lentiviral Infection. Lentiviral particle delivery technique was/were employed to infect adult DRG neurons with lentiviral plasmid DNA or shRNA. Production of lentiviral particles was conducted using the second-generation packaging system as previously described (J. Liu, S. et al., 2014). In brief, HEK293T cells were co-transfected with lentiviral plasmid DNA or shRNA and the packaging vectors pLP1, pLP2, and pLP-VSV-G (Thermo Fisher) using the calcium phosphate transfection method. At 24, 36, and 48 h after transfection, the virus-containing supernatant was collected, and the lentiviral particles concentrated (800-fold) by ultracentrifugation (100,000 × g at 4 °C for 2 h) prior to aliquoting and storage at -80 °C.

Plasmid DNA and shRNA. Lentiviral pVL-MitoDsRed and Lamp1-mRFP-FLAG were purchased from Addgene (cat. 44386, 34611).

Mitochondria and Lysosome Motility Assays. Dissociated adult DRG neurons were transduced at 24 h after plating with Mito-DsRed and/or Lamp1-mRFP-FLAG lentiviruses to track respectively mitochondria and lysosome motility. At 5 DIV, time-lapse images of neuron were acquired with 60× PlanApo objective lens (NA 1.4) and DS-Qi2 camera (Nikon) on Nikon Eclipse Ti microscope controlled by Nikon NIS-Elements software. During the image, neuron culture was incubated at 37 °C and 5% CO2 with Tokai Hit stage incubator. Proximal regions of intact axons (within 100 μm from the cell body) were selected for imaging, and time-lapse images were acquired at 2 s/frame for 10 min to track mitochondria and lysosomes. Kymographs were generated manually with a Fiji's plugin by tracing the proximal axon using a segmented line tool. Mitochondria and lysosome dynamic states were identified on kymographs and classified as follows: lysosomes and mitochondria were defined as stationary (ST) if fixed in an immobile state for the entire length of the movie. Dynamic mitochondria or lysosomes were subclassified as dynamic pausing, if showing persistent and short oscillatory movements in either direction (approximately <2 μm), or AR and RR running if moving for short or longer distances in either direction (approximately >2 μm). The number of different movement states per movie was scored and quantified on kymographs. The density of each dynamic state was reported as a percentage of total density to normalize for fluctuations in total numbers (Pero ME et al., 2021; Shin GJ et al., 2021).

Randomization and Blinding. Animals were randomly assigned to experimental groups to minimize allocation bias. Behavioral assessments and histological quantifications, including intraepidermal nerve fiber density measurements, were performed by investigators blinded to treatment allocation. Immunofluorescence images were analyzed using coded samples to minimize observer bias. Blinding was not systematically implemented during all experimental procedures or statistical analyses. Nevertheless, standardized experimental protocols and predefined analysis criteria were consistently applied across experimental groups to minimize potential bias.

Statistical analysis

Statistical analyses were performed using GraphPad Prism software (GraphPad Software, Boston, MA, USA). Data distribution was assessed using the Shapiro -Wilk normality test, and homogeneity of variances was evaluated using the Brown-Forsythe test, when applicable. Data are presented as mean ± standard deviation (SD), unless otherwise specified. Individual data points represent animals, independent biological experiments, neurites, or axons, depending on the experimental design, as specified in the corresponding figure legends. For comparisons between two independent groups, two-tailed unpaired Student's t-tests, Welch's t-tests, or Mann-Whitney U tests were used, as appropriate. For comparisons involving more than two independent groups, ordinary one-way analysis of variance (ANOVA) followed by Dunnett's multiple-comparisons test, Welch's ANOVA followed by Dunnett's T3 multiple-comparisons test, or the Kruskal-Wallis test followed by Dunn's multiple-comparisons test was performed, depending on data distribution and variance homogeneity. For repeated-measures datasets, the Friedman test followed by Dunn's multiple-comparisons test was used when appropriate. In the presence of missing repeated measurements, a mixed-effects model fitted using restricted maximum likelihood (REML) was applied, followed by Dunnett's multiple-comparisons test. Statistical analyses were performed separately for each experimental outcome and time point, as appropriate. The number of independent biological replicates, the experimental unit, and the statistical tests used are specified in the corresponding figure legends. For Kruskal-Wallis analyses, post hoc comparisons were interpreted as statistically significant only when the overall test reached significance. Exact p-values are reported whenever possible, with adjusted p-values provided for post hoc multiple comparisons. Statistical significance was defined as $p < 0.05$.

Author Contributions

F.B., G.C. C.M., S.G. and M.E.P., conceptualization, supervision, funding acquisition, project administration, review and editing the final manuscript. MEP and FB wrote the manuscript. M.E.P. and F.B. formal analysis, data curation, visualization. M.E.P. methodology, primary cell culture preparation, performed the in vitro degeneration assays, membrane potential evaluation, mitochondrial and lysosomal live-cell imaging, in vivo immunofluorescence analyses (with F.C.), in vitro tubulin PTM immunoblotting (with C.L.), seahorse metabolic analyses (with P.M.), and contributed to the interpretation of all experimental data. S.G. performed TBARS measurements (with S.D.), qPCR analyses, and OXPHOS protein analyses and formal analysis. C.M., E.P., A.C., A.C., V.A.C., performed the in vivo behavioral assessments and intraepidermal nerve fiber (IENF) density analyses. P.A. performed the electrophysiological studies. P.M. contributed to seahorse metabolic analyses. F.C. contributed to the in vivo immunofluorescence analyses. C.L. contributed to the in vitro tubulin PTM immunoblot analyses. P.L. and S.D.contributed to review and editing.

Funding
This work was supported by the Italian Ministry of University and Research (MIUR) under the PRIN grant 2017FJC3-004, awarded to G.C., S.G., and M.E.P., and by the National Institutes of Health (NIH) under grants R01CA279401A and RF1AG050658, awarded to F.B.
P.M. acknowledges funding from ARISTOS, which has received funding from the European Union's Horizon Europe research and innovation programme under the Marie Skłodowska-Curie grant agreement No. 101081334.

Declaration of Competing Interest
The authors declare that they have no known competing financial interests or personal relationships that could have appeared to influence the work reported in this paper.

Data Availability
The raw data of the study are archived and available at https://doi.org/10.17632/pfb2cwpt5x.2

References

1. Aguilar Diaz De Leon J, Borges CR. (2020). Evaluation of Oxidative Stress in Biological Samples Using the Thiobarbituric Acid Reactive Substances Assay. J Vis Exp. May 12;(159):10.3791/61122. doi: 10.3791/61122.
2. Argyriou AA, Cavaletti G, Briani C, Velasco R, Bruna J, Campagnolo M, Alberti P, Bergamo F, Cortinovis D, Cazzaniga M, Santos C, Papadimitriou K, Kalofonos HP. Clinical pattern and associations of oxaliplatin acute neurotoxicity: a prospective study in 170 patients with colorectal cancer. Cancer. 2013 Jan 15;119(2):438-44. doi: 10.1002/cncr.27732. Epub 2012 Jul 11. PMID: 22786764.
3. Apodaca G. Endocytic traffic in polarized epithelial cells: role of the actin and microtubule cytoskeleton. Traffic. 2001 Mar;2(3):149-59. doi: 10.1034/j.1600-0854.2001.020301. x. PMID: 11260520.
4. Argyriou AA, Velasco R, Briani C, Cavaletti G, Bruna J, Alberti P, Cacciavillani M, Lonardi S, Santos C, Cortinovis D, Cazzaniga M, Kalofonos HP. Peripheral neurotoxicity of oxaliplatin in combination with 5-fluorouracil (FOLFOX) or capecitabine (XELOX): a prospective evaluation of 150 colorectal cancer patients. Ann Oncol. 2012 Dec;23(12):3116-3122. doi: 10.1093/annonc/mds208. Epub 2012 Aug 2. PMID: 22865779.
5. Bart F. Werbrouck, Walter J. Pauwels & Jan L. De Bleecker. A case of 5-fluorouracil-induced peripheral neuropathy. Clinical Toxicology (2008) 46, 264-266.
6. Bennett GJ, Doyle T, Salvemini D. Mitotoxicity in distal symmetrical sensory peripheral neuropathies. Nat Rev Neurol. 2014 Jun;10(6):326-36. doi: 10.1038/nrneurol.2014.77. Epub 2014 May 20. Erratum in: Nat Rev Neurol. Aug;10(8):428. PMID: 24840972; PMCID: PMC4870000.

7. Bodakuntla S, Jijumon AS, Villablanca C, Gonzalez-Billault C, Janke C. Microtubule-Associated Proteins: Structuring the Cytoskeleton. Trends Cell Biol. 2019 Oct;29(10):804-819. doi: 10.1016/j.tcb.2019.07.004. Epub 2019 Aug 12. PMID: 31416684.
8. Bosc L, Pero ME, Balayssac D, Jacquemot N, Allard J, Suzanne P, Vollaire J, Cottet-Rousselle C, Michallet S, Villaret J, Torch S, Marais S, Elena-Herrmann B, Schlattner U, Mercier A, Josserand V, Thibert C, Dallemagne P, Bartolini F, Lafanechere L. Preventing neuropathy and improving anticancer chemotherapy with a carbazole-based compound. Sci Adv. 2025 Oct 31;11(44): eadw6328. doi: 10.1126/sciadv.adw6328. Epub 2025 Oct 29. PMID: 41160692; PMCID: PMC12571071.
9. Canta A, Chiorazzi A, Pozzi E, Fumagalli G, Monza L, Meregalli C, Carozzi VA, Rodriguez-Menendez V, Oggioni N, Näsström J, Marmiroli P, Cavaletti G. Calmangafodipir Reduces Sensory Alterations and Prevents Intraepidermal Nerve Fibers Loss in a Mouse Model of Oxaliplatin Induced Peripheral Neurotoxicity. Antioxidants (Basel). 2020 Jul 7;9(7):594. doi: 10.3390/antiox9070594. PMID: 32645985; PMCID: PMC7402145.
10. Canta A, Pozzi E, Carozzi VA. Mitochondrial Dysfunction in Chemotherapy-Induced Peripheral Neuropathy (CIPN). Toxics. 2015 Jun 5;3(2):198-223. doi: 10.3390/toxics3020198. PMID: 29056658; PMCID: PMC5634687.
11. Canta, A. Chiorazzi, G. Cavaletti, Tubulin: A target for antineoplastic drugs into the cancer cells but also in the peripheral nervous system. Curr. Med. Chem. 16, 1315-1324 (2009).
12. Cavaletti G, Alberti P, Frigeni B, Piatti M, Susani E. Chemotherapy-induced neuropathy. Curr Treat Options Neurol. 2011 Apr;13(2):180-90. doi: 10.1007/s11940-010-0108-3. PMID: 21191824.
13. Cavaletti G, Jakubowiak AJ. Peripheral neuropathy during bortezomib treatment of multiple myeloma: a review of recent studies. Haematologica. 2010 Feb;95(2):311-319. doi:10.3324/haematol.2009.015396. PMID: 20139392.
14. Cavaletti G, Marmiroli P. Chemotherapy-induced peripheral neurotoxicity. Nat Rev Neurol. 2010 Dec;6(12):657-66. doi: 10.1038/nrneurol.2010.160. Epub 2010 Nov 9. PMID: 21060341.
15. Chang DT, Reynolds IJ. Mitochondrial trafficking and morphology in healthy and injured neurons. Prog Neurobiol. 2006 Dec;80(5):241-68. doi: 10.1016/j.pneurobio.2006.09.003. Epub 2006 Dec 26. PMID: 17188795.
16. Chua KC, El-Haj N, Priotti J, Kroetz DL. Mechanistic insights into the pathogenesis of microtubule-targeting agent-induced peripheral neuropathy from pharmacogenetic and functional studies. Basic Clin Pharmacol Toxicol. 2022 Jan;130 Suppl 1(Suppl 1):60-74. doi: 10.1111/bcpt.13654. Epub 2021 Oct 2. PMID: 34481421; PMCID: PMC8716520.
17. Cordier PY, Nau A, Ciccolini J, Oliver M, Mercier C, Lacarelle B, Peytel E. 5-FU-induced neurotoxicity in cancer patients with profound DPD deficiency syndrome: a report of two cases. Cancer Chemother Pharmacol. 2011 Sep;68(3):823-6. doi: 10.1007/s00280-011-1666-0. Epub 2011 May 8. PMID: 21553285.
18. Detmer SA, Chan DC. Functions and dysfunctions of mitochondrial dynamics. Nat Rev Mol Cell Biol. 2007 Nov;8(11):870-9. doi: 10.1038/nrm2275. PMID: 17928812.
19. Doyle TM, Janes K, Xiao WH, Kolar GR, Luecke HF, Gratton MA, Tosh DK, Jacobson KA, Bennett GJ, Salvemini D. Mitochondrial A_3 Adenosine Receptor as a Mechanism for the Protective Effects of A_3AR Agonists on Chemotherapy-Induced Neuropathic Pain. J Neurosci. 2025 Jan 15;45(3):e1268242024. doi: 10.1523/JNEUROSCI.1268-24.2024. PMID: 39653498; PMCID: PMC11735668.
20. Doyle TM, Salvemini D. Mini-Review: Mitochondrial dysfunction and chemotherapy-induced neuropathic pain. Neurosci Lett. 2021 Aug 24; 760:136087. doi: 10.1016/j.neulet.2021.136087. Epub 2021 Jun 26. PMID: 34182057; PMCID: PMC9260825.
21. Ferguson SM. Axonal transport and maturation of lysosomes. Curr Opin Neurobiol. 2018 Aug;51:45-51. doi: 10.1016/j.conb.2018.02.020. Epub 2018 Mar 9. PMID: 29529416; PMCID: PMC6066426.

22. Flatters S.J.L, G.J. Bennett. Studies of peripheral sensory nerves in paclitaxel-induced painful peripheral neuropathy: Evidence for mitochondrial dysfunction. Pain, 122 (3) (2006), pp. 245-257
23. Flatters SJ. The contribution of mitochondria to sensory processing and pain. Prog Mol Biol Transl Sci. 2015;131:119-46. doi: 10.1016/bs.pmbts.2014.12.004. Epub 2015 Feb 7. PMID: 25744672.
24. Gamelin L, Gamelin E, Bossi L, Quasthoff S. Clinical aspects and molecular basis of oxaliplatin neurotoxicity: current management and development of preventive measures. Ann Oncol. 2002 Oct;13(10):1781-1791. doi:10.1093/annonc/mdf276. PMID: 12377646.
25. Geisler S, Doan RA, Strickland A, Huang X, Milbrandt J, DiAntonio A. Prevention of vincristine-induced peripheral neuropathy by genetic deletion of SARM1 in mice. Brain. 2016 Dec;139(Pt 12):3092-3108. doi: 10.1093/brain/aww251. Epub 2016 Oct 25. PMID: 27797810; PMCID: PMC5840884.
26. Geisler S., et al., Gene therapy targeting SARM1 blocks pathological axon degeneration in mice. J. Exp. Med. 216, 294–303 (2019).
27. Giatti S, Rigolio R, Romano S, Mitro N, Viviani B, Cavaletti G, Caruso D, Garcia-Segura LM, Melcangi RC. Dihydrotestosterone as a Protective Agent in Chronic Experimental Autoimmune Encephalomyelitis. Neuroendocrinology. 2015;101(4):296-308. doi: 10.1159/000381064. Epub 2015 Feb 26. PMID: 25765436.
28. Glimelius B, Manojlovic N, Pfeiffer P, Mosidze B, Kurteva G, Karlberg M, Mahalingam D, Buhl Jensen P, Kowalski J, Bengtson M, Nittve M, Näsström J. Persistent prevention of oxaliplatin-induced peripheral neuropathy using calmangafodipir (PledOx®): a placebo-controlled randomised phase II study (PLIANT). Acta Oncol. 2018 Mar;57(3):393-402. doi: 10.1080/0284186X.2017.1398836. Epub 2017 Nov 15. PMID: 29140155.
29. Gornstein, E. L. & Schwarz, T. L. Neurotoxic mechanisms of paclitaxel are local to the distal axon and independent of transport defects. Exp Neurol 288, 153-166, doi:10.1016/j.expneurol.2016.11.015 (2017).
30. Goshima, Y., Hida, T. & Gotoh, T. Computational analysis of axonal transport: a novel assessment of neurotoxicity, neuronal development and functions. Int J Mol Sci 13, 3414-3430, doi:10.3390/ijms13033414 (2012).
31. Grothey A. Oxaliplatin-safety profile: neurotoxicity. Clin Colorectal Cancer. 2003 Nov;3 Suppl 1:S38-46. doi:10.3816/CCC.2003.s.0013. PMID: 14523792.
32. Hershman DL, Unger JM, Crew KD, Minasian LM, Awad D, Moinpour CM, Hansen L, Lew DL, Greenlee H, Fehrenbacher L, Wade JL 3rd, Wong SF, Hortobagyi GN, Meyskens FL, Albain KS. Randomized double-blind placebo-controlled trial of acetyl-L-carnitine for the prevention of taxane-induced neuropathy in women undergoing adjuvant breast cancer therapy. J Clin Oncol. 2013 Jul 10;31(20):2627-33. doi: 10.1200/JCO.2012.44.8738. Epub 2013 Jun 3. PMID: 23733756; PMCID: PMC3699727.
33. Horibata S, Mahalingan KK, Patel R, Fan Y, Hotz JM, Ponton-Almodovar A, MacRenaris K, Li Y, Meerzaman D, Gottesman MM, Roll-Mecak A. Cisplatin resistance in an ovarian cancer model is mediated by microtubule dynamics regulator TPPP3 in synergy with tubulin code rewiring. Cell Rep. 2026 Jun 23;45(6):117414. doi: 10.1016/j.celrep.2026.117414. Epub 2026 Jun 4. PMID: 42241284.
34. Iseppon F, Malacrida A, Chiorazzi A, Canta A, Alberti P, Carozzi VA, Pozzi E, Rodriguez-Menendez V, Cherchi L, Fabbro V, Pagani L, Tonelli E, Tapella L, Mattarei A, Palermo S, Cartelli D, Mauri M, Scimia N, Stanga S, Lim D, Distasi C, Delconti M, Chinello C, Morcillo P, Pero ME, Bartolini F, Cavaletti G, Meregalli C. Shared and specific molecular mechanisms of proteasome inhibitors in chemotherapy-induced peripheral neurotoxicity. Br J Pharmacol. 2026 May 28. doi: 10.1111/bph.70501. Epub ahead of print. PMID: 42206739.
35. Lucchetta M, Lonardi S, Bergamo F, Alberti P, Velasco R, Argyriou AA, Briani C, Bruna J, Cazzaniga M, Cortinovis D, Cavaletti G, Kalofonos HP. Incidence of atypical acute nerve

hyperexcitability symptoms in oxaliplatin-treated patients with colorectal cancer. Cancer Chemother Pharmacol. 2012 Dec;70(6):899-902. doi: 10.1007/s00280-012-2006-8. Epub 2012 Oct 30. PMID: 23108696.
36. Janke C, Magiera MM. The tubulin code and its role in controlling microtubule properties and functions. Nat Rev Mol Cell Biol. 2020 Jun;21(6):307-326. doi: 10.1038/s41580-020-0214-3. Epub 2020 Feb 27. PMID: 32107477.
37. Janke C, Rogowski K, Wloga D, Regnard C, Kajava AV, Strub JM, Temurak N, van Dijk J, Boucher D, van Dorsselaer A, Suryavanshi S, Gaertig J, Eddé B. Tubulin polyglutamylase enzymes are members of the TTL domain protein family. Science. 2005 Jun 17;308(5729):1758-62. doi: 10.1126/science.1113010. Epub 2005 May 12. PMID: 15890843.
38. Karlsson JOG, Jynge P, Ignarro LJ. Exacerbated Neuropathy in POLAR A and M Trials Due to Redox Interaction of PledOx-Associated Mn^{2+} and Oxaliplatin-Associated Pt^{2}. Antioxidants (Basel). 2023 Mar 1;12(3):608. doi: 10.3390/antiox12030608. PMID: 36978857; PMCID: PMC10045419.
39. Leandro-Garcia, L. J. et al. Regulatory polymorphisms in beta-tubulin IIa are associated with paclitaxel-induced peripheral neuropathy. Clin Cancer Res 18, 4441-4448, doi:10.1158/1078-0432.CCR-12-1221 (2012).
40. Li Y, Huang Y, Zhang Y, et al. Risk factors of paclitaxel-induced peripheral neuropathy. Front Oncol. 2024; 14:1327318. doi:10.3389/fonc.2024.1327318. Link.
41. Ma J, Kavelaars A, Dougherty PM, Heijnen CJ. Beyond symptomatic relief for chemotherapy-induced peripheral neuropathy: Targeting the source. Cancer. 2018 Jun 1;124(11):2289-2298. doi: 10.1002/cncr.31248. Epub 2018 Feb 20. PMID: 29461625; PMCID: PMC5991994.
42. Malacrida A, Meregalli C, Rodriguez-Menendez V, Nicolini G. Chemotherapy-Induced Peripheral Neuropathy and Changes in Cytoskeleton. Int J Mol Sci. 2019 May 9;20(9):2287. doi: 10.3390/ijms20092287. PMID: 31075828; PMCID: PMC6540147.
43. Marmiroli P, Riva B, Pozzi E, Ballarini E, Lim D, Chiorazzi A, Meregalli C, Distasi C, Renn CL, Semperboni S, Morosi L, Ruffinatti FA, Zucchetti M, Dorsey SG, Cavaletti G, Genazzani A, Carozzi VA. Susceptibility of different mouse strains to oxaliplatin peripheral neurotoxicity: Phenotypic and genotypic insights. PLoS One. 2017 Oct 11;12(10):e0186250. doi: 10.1371/journal.pone.0186250. PMID: 29020118; PMCID: PMC5636145.
44. Martínez-Hernández J, Parato J, Sharma A, Soleilhac JM, Qu X, Tein E, Sproul A, Andrieux A, Goldberg Y, Moutin MJ, Bartolini F, Peris L. Crosstalk between acetylation and the tyrosination/detyrosination cycle of α-tubulin in Alzheimer's disease. Front Cell Dev Biol. 2022 Aug 26;10:926914. doi: 10.3389/fcell.2022.926914. PMID: 36092705; PMCID: PMC9459041.
45. Marullo R, Werner E, Degtyareva N, Moore B, Altavilla G, Ramalingam SS, Doetsch PW. Cisplatin induces a mitochondrial-ROS response that contributes to cytotoxicity depending on mitochondrial redox status and bioenergetic functions. PLoS One. 2013 Nov 19;8(11):e81162. doi: 10.1371/journal.pone.0081162. PMID: 24260552; PMCID: PMC3834214.
46. Meregalli C, Monza L, Jongen JLM. A mechanistic understanding of the relationship between skin innervation and chemotherapy-induced neuropathic pain. Front Pain Res (Lausanne). 2022 Dec 13;3:1066069. doi: 10.3389/fpain.2022.1066069. PMID: 36582196; PMCID: PMC9792502.
47. Meregalli, C. et al. Evaluation of tubulin polymerization and chronic inhibition of proteasome as citotoxicity mechanisms in bortezomib-induced peripheral neuropathy. Cell Cycle 13, 612-621, doi:10.4161/cc.27476 (2014).
48. Morcillo P, Kabra K, Velasco K, Cordero H, Jennings S, Yun TD, Larrea D, Akman HO, Schon EA. Aberrant ER-mitochondria communication is a common pathomechanism in mitochondrial disease. Cell Death Dis. 2024 Jun 10;15(6):405. doi: 10.1038/s41419-024-06781-9. PMID: 38858390; PMCID: PMC11164949.
49. Moreau P, Pylypenko H, Grosicki S, Karamanesht I, Leleu X, Grishunina M, Rekhtman G, Masliak Z, Robak T, Shubina A, Arnulf B, Kropff M, Cavet J, Esseltine DL, Feng H, Girgis S, Harousseau JL; PX-171-009 Investigators. Subcutaneous versus intravenous administration of

bortezomib in patients with relapsed multiple myeloma: a randomised, phase 3, non-inferiority study. J Clin Oncol. 2011 May 20;29(15):1911-1917. doi:10.1200/JCO.2010.33.4931. PMID: 21444867.
50. Mullen RJ, Eicher EM, Sidman RL. Purkinje cell degeneration, a new neurological mutation in the mouse. Proc Natl Acad Sci U S A. 1976 Jan;73(1):208-12. doi: 10.1073/pnas.73.1.208. PMID: 1061118; PMCID: PMC335870.
51. Nunnari J, Suomalainen A. Mitochondria: in sickness and in health. Cell. 2012 Mar 16;148(6):1145-59. doi: 10.1016/j.cell.2012.02.035. PMID: 22424226; PMCID: PMC5381524.
52. Park SB, Cetinkaya-Fisgin A, Argyriou AA, Höke A, Cavaletti G, Alberti P. Axonal degeneration in chemotherapy-induced peripheral neurotoxicity: clinical and experimental evidence. J Neurol Neurosurg Psychiatry. 2023 Nov;94(11):962-972. doi: 10.1136/jnnp-2021-328323. Epub 2023 Apr 4. PMID: 37015772; PMCID: PMC10579520.
53. Park SB, Goldstein D, Krishnan AV, Lin CS, Friedlander ML, Cassidy J, Koltzenburg M, Kiernan MC. Chemotherapy-induced peripheral neurotoxicity: a critical analysis. CA Cancer J Clin. 2013 Nov-Dec;63(6):419-37. doi: 10.3322/caac.21204. PMID: 24590861.
54. Qu X, Yuan FN, Corona C, Pasini S, Pero ME, Gundersen GG, Shelanski ML, Bartolini F. Stabilization of dynamic microtubules by mDia1 drives Tau-dependent $A\beta_{1-42}$ synaptotoxicity. J Cell Biol. 2017 Oct 2;216(10):3161-3178. doi: 10.1083/jcb.201701045. Epub 2017 Sep 6. PMID: 28877993; PMCID: PMC5626542.
55. Peris L, Parato J, Qu X, Soleilhac JM, Lanté F, Kumar A, Pero ME, Martínez-Hernández J, Corrao C, Falivelli G, Payet F, Gory-Fauré S, Bosc C, Blanca Ramirez M, Sproul A, Brocard J, Di Cara B, Delagrange P, Buisson A, Goldberg Y, Moutin MJ, Bartolini F, Andrieux A. Tubulin tyrosination regulates synaptic function and is disrupted in Alzheimer's disease. Brain. 2022 Jul 29;145(7):2486-2506. doi: 10.1093/brain/awab436. PMID: 35148384; PMCID: PMC9337816.
56. Pero ME, Chowdhury F, Bartolini F. Role of tubulin post-translational modifications in peripheral neuropathy. Exp Neurol. 2023 Feb;360:114274. doi: 10.1016/j.expneurol.2022.114274. Epub 2022 Nov 13. PMID: 36379274; PMCID: PMC11320756.
57. Pero ME, Meregalli C, Qu X, Shin GJ, Kumar A, Shorey M, Rolls MM, Tanji K, Brannagan TH, Alberti P, Fumagalli G, Monza L, Grueber WB, Cavaletti G, Bartolini F. Pathogenic role of delta 2 tubulin in bortezomib-induced peripheral neuropathy. Proc Natl Acad Sci U S A. 2021 Jan 26;118(4):e2012685118. doi: 10.1073/pnas.2012685118. Erratum in: Proc Natl Acad Sci U S A. 2021 Nov 9;118(45):e2115637118. doi: 10.1073/pnas.2115637118. PMID: 33468672; PMCID: PMC7848563.
58. Pfeiffer P, Lustberg M, Nässtrom J, Carlsson S, Persson A, Nagahama F, Cavaletti G, Glimelius B, Muro K. Calmangafodipir for Prevention of Oxaliplatin-Induced Peripheral Neuropathy: Two Placebo-Controlled, Randomized Phase 3 Studies (POLAR-A/POLAR-M). JNCI Cancer Spectr. 2022 Nov 1;6(6):pkac075. doi: 10.1093/jncics/pkac075. PMID: 36308441; PMCID: PMC9678401.
59. Pfeiffer P, Lustberg M, Nässtrom J, Carlsson S, Persson A, Nagahama F, Cavaletti G, Glimelius B, Muro K. Calmangafodipir for Prevention of Oxaliplatin-Induced Peripheral Neuropathy: Two Placebo-Controlled, Randomized Phase 3 Studies (POLAR-A/POLAR-M). JNCI Cancer Spectr. 2022 Nov 1;6(6):pkac075. doi: 10.1093/jncics/pkac075. PMID: 36308441; PMCID: PMC9678401
60. Pozzi E, Ballarini E, Rodriguez-Menendez V, Canta A, Chiorazzi A, Monza L, Bossi M, Alberti P, Malacrida A, Meregalli C, et al. Paclitaxel, but Not Cisplatin, Affects Satellite Glial Cells in Dorsal Root Ganglia of Rats with Chemotherapy-Induced Peripheral Neurotoxicity. Toxics. 2023; 11(2):93. https://doi.org/10.3390/toxics11020093
61. Pu J, Guardia CM, Keren-Kaplan T, Bonifacino JS. Mechanisms and functions of lysosome positioning. J Cell Sci. 2016 Dec 1;129(23):4329-4339. doi: 10.1242/jcs.196287. Epub 2016 Oct 31. PMID: 27799357; PMCID: PMC5201012.

62. Rogowski K, van Dijk J, Magiera MM, Bosc C, Deloulme JC, Bosson A, Peris L, Gold ND, Lacroix B, Bosch Grau M, Bec N, Larroque C, Desagher S, Holzer M, Andrieux A, Moutin MJ, Janke C. A family of protein-deglutamylating enzymes associated with neurodegeneration. Cell. 2010 Nov 12;143(4):564-78. doi: 10.1016/j.cell.2010.10.014. PMID: 21074048.
63. Russell, J. W., Windebank, A. J., McNiven, M. A., Brat, D. J. & Brimijoin, W. S. Effect of cisplatin and ACTH4-9 on neural transport in cisplatin induced neurotoxicity. Brain Res 676, 258-267 (1995).
64. Seretny M, Currie GL, Sena ES, Ramnarine S, Grant R, MacLeod MR, Colvin LA, Fallon M. Incidence, prevalence, and predictors of chemotherapy-induced peripheral neuropathy: A systematic review and meta-analysis. Pain. 2014 Dec;155(12):2461-2470. doi: 10.1016/j.pain.2014.09.020. PMID: 25261162.
65. Settembre C, Fraldi A, Medina DL, Ballabio A. Signals from the lysosome: a control centre for cellular clearance and energy metabolism. Nat Rev Mol Cell Biol. 2013 May;14(5):283-96. doi: 10.1038/nrm3565. PMID: 23609508; PMCID: PMC4387238.
66. Shashi V, Magiera MM, Klein D, Zaki M, Schoch K, Rudnik-Schöneborn S, Norman A, Lopes Abath Neto O, Dusl M, Yuan X, Bartesaghi L, De Marco P, Alfares AA, Marom R, Arold ST, Guzmán-Vega FJ, Pena LD, Smith EC, Steinlin M, Babiker MO, Mohassel P, Foley AR, Donkervoort S, Kaur R, Ghosh PS, Stanley V, Musaev D, Nava C, Mignot C, Keren B, Scala M, Tassano E, Picco P, Doneda P, Fiorillo C, Issa MY, Alassiri A, Alahmad A, Gerard A, Liu P, Yang Y, Ertl-Wagner B, Kranz PG, Wentzensen IM, Stucka R, Stong N, Allen AS, Goldstein DB; Undiagnosed Diseases Network; Schoser B, Rösler KM, Alfadhel M, Capra V, Chrast R, Strom TM, Kamsteeg EJ, Bönnemann CG, Gleeson JG, Martini R, Janke C, Senderek J. Loss of tubulin deglutamylase CCP1 causes infantile-onset neurodegeneration. EMBO J. 2018 Dec 3;37(23):e100540. doi: 10.15252/embj.2018100540. Epub 2018 Nov 12. PMID: 30420557; PMCID: PMC6276871.
67. Shin GJ, Pero ME, Hammond LA, Burgos A, Kumar A, Galindo SE, Lucas T, Bartolini F, Grueber WB. Integrins protect sensory neurons in models of paclitaxel-induced peripheral sensory neuropathy. Proc Natl Acad Sci U S A. 2021 Apr 13;118(15):e2006050118. doi: 10.1073/pnas.2006050118. PMID: 33876743; PMCID: PMC8053987.
68. Sirajuddin M, Rice LM, Vale RD. Regulation of microtubule motors by tubulin isotypes and post-translational modifications. Nat Cell Biol. 2014 Apr;16(4):335-44. doi: 10.1038/ncb2920. Epub 2014 Mar 16. PMID: 24633327; PMCID: PMC4117587.
69. Staff NP, Podratz JL, Grassner L, Bader M, Paz J, Knight AM, Loprinzi CL, Trushina E, Windebank AJ. Bortezomib alters microtubule polymerization and axonal transport in rat dorsal root ganglion neurons. Neurotoxicology. 2013 Dec; 39:124-31. doi: 10.1016/j.neuro.2013.09.001. Epub 2013 Sep 12. PMID: 24035926; PMCID: PMC3844018.
70. Spinelli JB, Haigis MC. The multifaceted contributions of mitochondria to cellular metabolism. Nat Cell Biol. 2018 Jul;20(7):745-754. doi: 10.1038/s41556-018-0124-1. Epub 2018 Jun 27. PMID: 29950572; PMCID: PMC6541229
71. Starobova H. and Vetter I. Pathophysiology of chemotherapy-induced peripheral neuropathy. Front Mol Neurosci. 2017 Jun 13;10:174. doi:10.3389/fnmol.2017.00174. PMID: 28620280.
72. Suomalainen A, Battersby BJ. Mitochondrial diseases: the contribution of organelle stress responses to pathology. Nat Rev Mol Cell Biol. 2018 Feb;19(2):77-92. doi: 10.1038/nrm.2017.66. Epub 2017 Aug 9. PMID: 28792006.
73. Susanto AC, Hartajanie L, Wu CC. Œ± Phellandrene enhances the apoptosis of HT 29 cells induced by 5 fluorouracil by modulating the mitochondria dependent pathway. Oncol Rep. 2024 Apr;51(4):61. doi: 10.3892/or.2024.8720. Epub 2024 Mar 8. PMID: 38456489; PMCID: PMC10940876.
74. Tarasiuk O, Chiorazzi A, Argentini A, Ballarini E, Canta A, Carozzi VA, Pozzi E, Alberti P, Fabbro V, Iseppon F, Foti M, Meregalli C. Interleukin-6 as a keystone cytokine in experimental

rat models of chemotherapy-induced peripheral neurotoxicity. Sci Rep. 2026 Jan 13;16(1):5127. doi: 10.1038/s41598-025-34830-6. PMID: 41530329; PMCID: PMC12876870.
75. Trecarichi A, Flatters SJL. Mitochondrial dysfunction in the pathogenesis of chemotherapy-induced peripheral neuropathy. Int Rev Neurobiol. 2019; 145:83-126. doi: 10.1016/bs.irn.2019.05.001. Epub 2019 Jun 6. PMID: 31208528.
76. van den Bent MJ, van Raaij-van den Aarssen VJ, Verweij J, Doorn PA, Sillevis Smitt PA. Progression of paclitaxel-induced neuropathy following discontinuation of treatment. Muscle Nerve. 1997 Jun;20(6):750-2. doi: 10.1002/(sici)1097-4598(199706)20:6<750::aid-mus15>3.0.co;2-y. PMID: 9149085.
77. Wallace DC. A mitochondrial bioenergetic etiology of disease. J Clin Invest. 2013 Apr;123(4):1405-12. doi: 10.1172/JCI61398. Epub 2013 Apr 1. PMID: 23543062; PMCID: PMC3614529.

78. Wozniak KM, Vornov JJ, Wu Y, Liu Y, Carozzi VA, Rodriguez-Menendez V, Ballarini E, Alberti P, Pozzi E, Semperboni S, Cook BM, Littlefield BA, Nomoto K, Condon K, Eckley S, DesJardins C, Wilson L, Jordan MA, Feinstein SC, Cavaletti G, Polydefkis M, Slusher BS. Peripheral Neuropathy Induced by Microtubule-Targeted Chemotherapies: Insights into Acute Injury and Long-term Recovery. Cancer Res. 2018 Feb 1;78(3):817-829. doi: 10.1158/0008-5472.CAN-17-1467. Epub 2017 Nov 30. PMID: 29191802; PMCID: PMC5811354.
79. Yuan W, Ji G, Shi X, Sun Z, Liu C, Yu Y, Li W, Wang X, Hu H. The male reproductive toxicity after 5-Fluorouracil exposure: DNA damage, oxidative stress, and mitochondrial dysfunction in vitro and in vivo. Ecotoxicol Environ Saf. 2024 Jun 15; 278:116465. doi: 10.1016/j.ecoenv.2024.116465. Epub 2024 May 14. PMID: 38749198.
80. Zheng H, Xiao WH, Bennett GJ. Functional deficits in peripheral nerve mitochondria in rats with paclitaxel- and oxaliplatin-evoked painful peripheral neuropathy. Exp Neurol. 2011 Dec;232(2):154-61. doi: 10.1016/j.expneurol.2011.08.016. Epub 2011 Aug 30. PMID: 21907196; PMCID: PMC3202047.
81. Wallace DC. A mitochondrial bioenergetic etiology of disease. J Clin Invest. 2013 Apr;123(4):1405-12. doi: 10.1172/JCI61398. Epub 2013 Apr 1. PMID: 23543062; PMCID: PMC3614529.

Supplementary Files

This is a list of supplementary files associated with this preprint. Click to download.

- uncroppedwesternblot.docx
- PeroMEetal.2026supplementaryfile.docx